NASA Contractor Report 3865

NASA-CR-3865 19850009981

An Implicit, Conservative, Zonal-Boundary Scheme for Euler Equation Calculations

Man Mohan Rai

CONTRACT NAS2-11555
FEBRUARY 1985

FOR REFERENCE

NOT TO BE TAKEN FROM THIS ROOM

[illegible] COPY

[illegible] LIBRARY
[illegible]
HAMPTON, VIRGINIA

NASA

NASA Contractor Report 3865

An Implicit, Conservative, Zonal-Boundary Scheme for Euler Equation Calculations

Man Mohan Rai
Informatics General Corporation
Palo Alto, California

Prepared for
Ames Research Center
under Contract NAS2-11555

National Aeronautics
and Space Administration

Scientific and Technical Information Branch

1985

AN IMPLICIT, CONSERVATIVE, ZONAL-BOUNDARY SCHEME FOR EULER EQUATION CALCULATIONS

Man Mohan Rai*

Ames Research Center

SUMMARY

A "zonal," or "patched," grid approach is one in which the flow region of interest is divided into subregions which are then discretized independently, using existing grid generators. The equations of motion are integrated in each subregion in conjunction with zonal-boundary schemes which allow proper information transfer across interfaces that separate subregions. The zonal approach greatly simplifies the treatment of complex geometries and also the addition of grid points to selected regions of the flow. In this study a conservative, zonal-boundary condition that could be used with explicit schemes has been extended so that it can be used with existing second-order-accurate implicit integration schemes such as the Beam-Warming and Osher schemes. In the test case considered, the implicit schemes increased the rate of convergence considerably (by a factor of about 30 over that of the explicit scheme). Results demonstrating the time-accuracy of the zonal scheme and the feasibility of performing calculations on zones that move relative to each other are also presented.

INTRODUCTION

A major problem in computational fluid dynamics is the generation of grids for realistic, three-dimensional bodies such as complete aircraft configurations. The generation of a single grid that discretizes the entire flow region associated with a complex configuration is extremely difficult and, for some problems, impractical. Often, an attempt to generate a single grid for a complicated flow region results in highly skewed grids which in turn result in inaccurate calculations; also, such an attempt usually requires an inordinate amount of the aerodynamicist's time to "tune" existing grid-generation schemes to yield acceptable grids. A second factor that contributes to the complexity of grid generation is the necessity to cluster grid points in regions where the dependent variables and their gradients change rapidly (selective grid refinement).

The problems mentioned above can be overcome to a limited extent by developing very sophisticated grid-generation schemes. However, an alternative approach is to divide the given region into simpler subregions such that each subregion (or zone) is a geometrically simple figure; for example, every two-dimensional region can be divided into simple four-sided zones and every three-dimensional region into six-sided zones. Grids can then be independently generated for each zone using existing grid-generation schemes. The zonal approach has the following advantages:

1. The grid for any arbitrary region can be generated in a simple, straightforward manner (since the zones are geometrically simple).

*Principal Analyst, Informatics General Corporation, Palo Alto, California.

2. Flow regions requiring grid refinement can be isolated in separate zones, and the required number of grid points can be introduced in these zones (if necessary this can be done adaptively as the solution progresses in time).

3. The zonal approach facilitates the use of different equation sets in different zones; hence, simpler equation sets can be used in certain regions of the flow. This may result in a saving of computer time.

4. The zonal approach also facilitates a block-processing scheme wherein only the data corresponding to certain regions of the flow field are required to reside in the main memory of the computer; the remaining data can be stored on disk or tape. Theoretically, the block-processing technique permits the use of unlimited global grid sizes (computing speeds become a limiting factor in this case).

The division of a given region into zones introduces new boundaries in the calculation: the zonal boundaries. Since the grid for each region is generated independently, the grid lines of two adjoining regions may align (continuous grids) or may not align (discontinuous grids) with each other. Even in the case of continuous grids, a sudden change in grid spacing or grid-line orientation across the zonal boundary may give rise to discontinuities in the transformation metrics (metric-discontinuous grids). Figure 1 shows the different types of grids mentioned above.

The following examples serve to illustrate some of the advantages of the zonal approach. Figure 2 shows the flow region associated with a combination of three airfoils. The region is multiply connected and hence difficult to discretize with a single grid system. The division of the flow field into 13 zones, as in figure 2, results in simple four-sided regions which can be discretized easily. Figure 3(a)

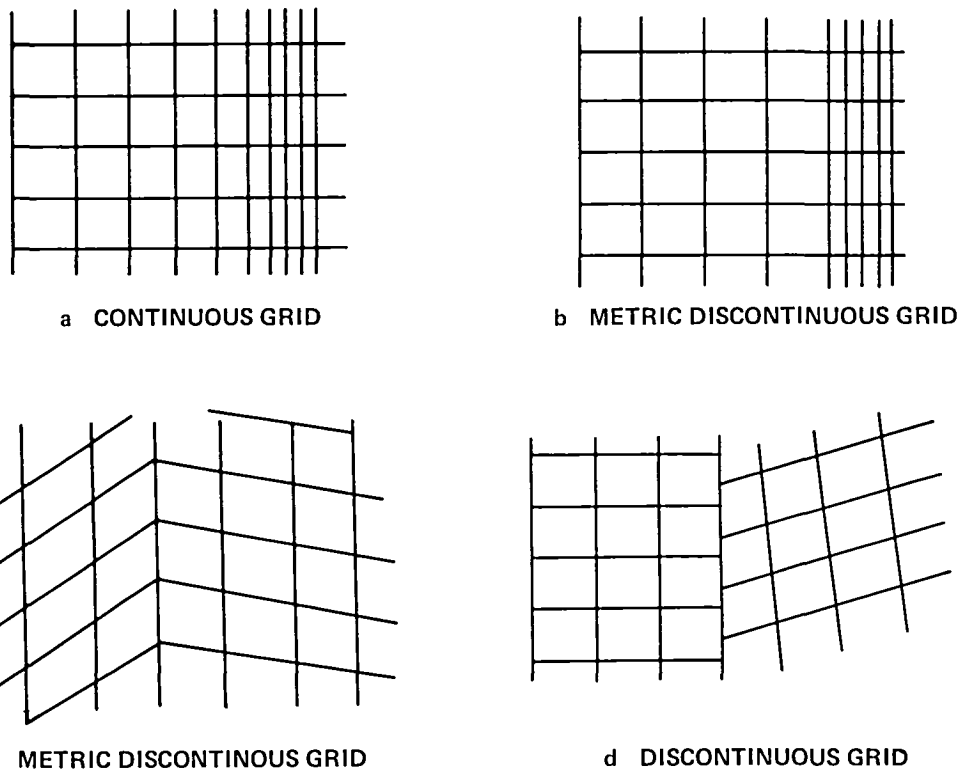

Fig. 1.- Types of grids used in finite-difference calculations. (a) Continuous. (b) Metric-discontinuous (abrupt change in grid line spacing). (c) Metric-discontinuous (abrupt change in grid-line orientation). (d) Discontinuous.

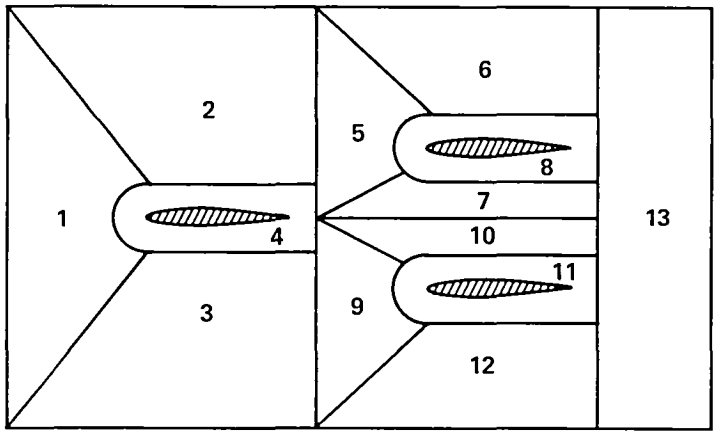

Figure 2.- Zoning of the multiply connected region associated with three airfoils.

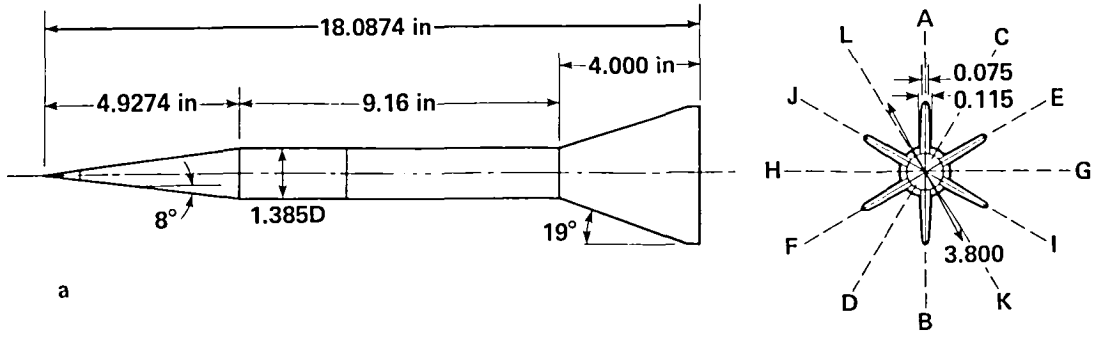

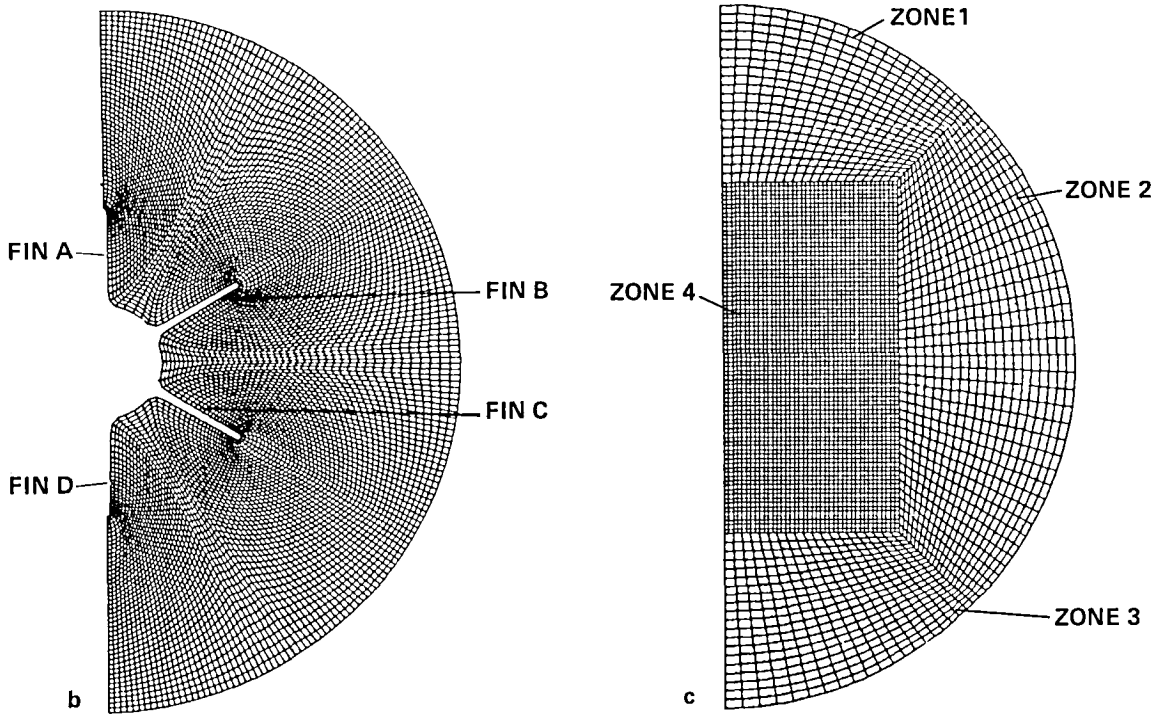

Figure 3.- Finned projectile. (a) Geometry of projectile. (b) Grid at the aft end (just before the body terminates). (c) Grid at the aft end (just after the body terminates).

shows a six-finned projectile, and figure 3(b) shows the grid used to discretize the flow region at the aft end of the projectile (ref. 1). Immediately after this axial station an entirely new type of grid (fig. 3(c)) is required because of the sudden termination of the body. This transition can be achieved by treating the plane corresponding to the aft end of the projectile as a two-dimensional (surface) zonal boundary separating two three-dimensional zones. It should be noted that the grid in figure 3(c) is itself composed of four two-dimensional grids separated by one-dimensional (line) zonal boundaries. The grids in figure 3(c) alleviate the geometric singularity problem associated with a simple polar grid and also facilitate the addition of grid points to the central portion of the flow region (to accurately model the wake).

In order that information be transferred from one zone to another accurately, it is important to treat grid points on the zonal boundaries with care. The nonlinear nature of the Euler and Navier-Stokes equations permits solutions with discontinuities, such as shocks. It is imperative that the finite-difference scheme used for the calculation be conservative so that these discontinuities, when captured, assume the right strength and physical location. In a zonal calculation, it is important that the zonal boundaries also be treated in a conservative manner so that the discontinuities can move freely across these boundaries. Results demonstrating the importance of maintaining conservation at zonal boundaries can be found in reference 2.

A fully conservative zonal-boundary scheme, which permits the movement of discontinuities across zonal boundaries with minimal distortion of the solution, is developed in reference 3. The scheme is designed for both discontinuous and metric-discontinuous grids and can be used in conjunction with first-order-accurate, explicit integration schemes. The scheme is stable, accurate, and is formulated in generalized coordinates. Results demonstrating these characteristics of the scheme are also presented in reference 3. The demonstration calculations include supersonic flow over a cylinder, blast-wave diffraction by a ramp, and the one-dimensional shock-tube problem solved on a two-dimensional grid.

The first-order-accurate schemes used in reference 3 are insufficient to produce accurate results for a general class of problems. Hence, it is necessary to extend the zonal scheme of reference 3 so that it can be used with second-order-accurate integration schemes. The purpose of extending the explicit zonal scheme to work in conjunction with implicit schemes is twofold. The first reason is the increase in convergence rates and the consequent reduction in computing costs that can be obtained with the implicit schemes. Calculations with the Navier-Stokes equations require very fine grids in viscously dominated regions (to accurately resolve flow properties) and relatively coarse grids in regions where viscous effects are negligible. Hence, mesh-cell areas in grids used for Navier-Stokes calculations can vary over several orders of magnitude. Navier-Stokes calculations with explicit schemes (with the attendant time-step restrictions) are impractical, and it is necessary to resort to implicit integration schemes. Since the ultimate objective of the zonal approach is to solve the unsteady Navier-Stokes equations in any given region, a first step in that direction is the implicitization of the zonal-boundary condition. The advantage of using an implicit scheme, however, is not restricted to viscous calculations. The convergence rate can be expected to improve even in inviscid calculations where the mesh-cell size varies widely. The second reason for the implicitization of the zonal scheme is that it can then be incorporated into a number of existing analysis codes that use implicit integration algorithms.

The present study deals with the changes required to extend the zonal scheme of reference 3 so that it can be used with first-order-accurate and second-order-accurate implicit schemes, in particular with the Beam-Warming scheme (ref. 4) and an implicit form of the Osher scheme (ref. 5). The implicit zonal scheme and the integration schemes used are described in the following sections. The zonal scheme is developed for the Euler equations cast in generalized coordinates.

Results are presented for a cylinder in a supersonic flow. This calculation demonstrates the conservative property of the zonal scheme and also the considerable increase in convergence rates that can be achieved with an implicit integration scheme coupled with an implicit zonal scheme (relative to explicit integration and zonal schemes). A second calculation, consisting of a cylinder in subsonic flow, is also included. The calculation is performed on two grids, one rotating and the other stationary. This calculation demonstrates the time-accuracy of the scheme and also the feasibility of performing calculations on multiple zones of which some are moving relative to others. Zonal calculations in which zones move relative to each other will be frequently required in applications where some parts of the system move with respect to other parts, for example, the rotor-fuselage combination of a helicopter, turbines, and propeller-nacelle configurations. Finally, results are presented for the motion of a Lamb-type vortex through a zonal boundary. Pressure contours corresponding to the vortex remain distortion-free as they move through the zonal boundary. Since the exact position of the center of the vortex is known at all times (the problem is formulated so that this information is known), this calculation can be used to test the time-accuracy of the zonal scheme. The time-accuracy obtained in this case was found to be good.

THE ZONAL-BOUNDARY SCHEME

The explicit form of the zonal-boundary scheme is described in detail in reference 3. In this section, the explicit zonal scheme is briefly outlined, and the necessary flux linearizations required to convert the scheme to an implicit scheme are then presented.

Review of the Explicit Zonal Scheme

Consider the unsteady Euler equations in two dimensions:

$$Q_t + E_x + F_y = 0 \tag{1}$$

The vectors Q, E, and F are given by

$$Q = \begin{bmatrix} \rho \\ \rho u \\ \rho v \\ e \end{bmatrix} \qquad E = \begin{bmatrix} \rho u \\ p + \rho u^2 \\ \rho uv \\ (e + p)u \end{bmatrix} \qquad F = \begin{bmatrix} \rho v \\ \rho uv \\ p + \rho v^2 \\ (e + p)v \end{bmatrix} \tag{2}$$

where ρ is the density; p is the pressure; u and v are the velocities in the x and y directions, respectively; and e is the total internal energy per unit volume:

$$e = \frac{p}{\gamma - 1} + \frac{\rho}{2}(u^2 + v^2) \tag{3}$$

Consider the two curvilinear grids used to discretize the flow region shown in figure 4. The line AB represents the zonal boundary that separates the two grids used to discretize the given region. Let ℓ and m be the indices used in the ξ and η directions, respectively, in zone 1, and let j and k be the corresponding indices for zone 2. Note that the notation used in this study is different from that used in reference 3 (m and k increase in opposite directions in ref. 3). Let n represent the time-step for both zones. A superscript within parentheses will denote the zone to which a given quantity belongs; for example, $\Delta\tau^{(1)}$ denotes the marching-step size in zone 1.

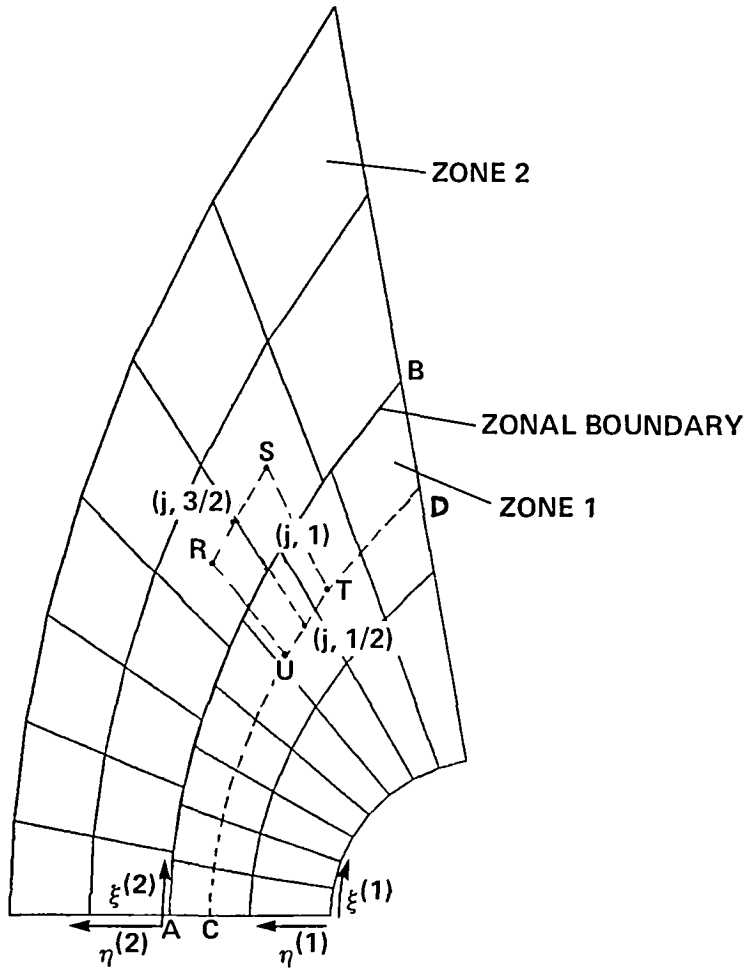

Figure 4.- Two-zone grid to illustrate zonal scheme in curvilinear coordinates.

Establishing two independent-variable transformations (one for each grid),

$$\left.\begin{aligned} \tau^{(i)} &= t \\ \xi^{(i)} &= \xi^{(i)}(x,y,t) \\ \eta^{(i)} &= \eta^{(i)}(x,y,t) \end{aligned}\right\} \qquad i = \begin{cases} 1 \text{ for zone 1} \\ 2 \text{ for zone 2} \end{cases} \tag{4}$$

and applying these transformations to equation (1), the following is obtained:

$$\tilde{Q}^{(i)}_{\tau^{(i)}} + \tilde{E}^{(i)}_{\xi^{(i)}} + \tilde{F}^{(i)}_{\eta^{(i)}} = 0 \qquad i = 1,2 \tag{5}$$

where

$$\left.\begin{aligned} \tilde{Q}^{(i)} &= Q/J^{(i)} \\ \tilde{E}^{(i)}(Q,\xi^{(i)}) &= [\xi_t^{(i)}Q + \xi_x^{(i)}E + \xi_y^{(i)}F]/J^{(i)} \\ \tilde{F}^{(i)}(Q,\eta^{(i)}) &= [\eta_t^{(i)}Q + \eta_x^{(i)}E + \eta_y^{(i)}F]/J^{(i)} \\ J^{(i)} &= \xi_x^{(i)}\eta_y^{(i)} - \eta_x^{(i)}\xi_y^{(i)} \end{aligned}\right\} \tag{6}$$

The notation $\tilde{E}^{(i)}(Q,\xi^{(i)})$ and $\tilde{F}^{(i)}(Q,\eta^{(i)})$ is used to show the dependence of these quantities on the metrics of the transformation. Let the conservative difference schemes used to integrate equation (5) be given by

$$\frac{\Delta\tilde{Q}^{(1)}_{\ell,m}}{\Delta\tau^{(1)}} + \frac{\hat{E}^{(1)}_{\ell+1/2,m} - \hat{E}^{(1)}_{\ell-1/2,m}}{\Delta\xi^{(1)}} + \frac{\hat{F}^{(1)}_{\ell,m+1/2} - \hat{F}^{(1)}_{\ell,m-1/2}}{\Delta\eta^{(1)}} = 0 \tag{7}$$

and

$$\frac{\Delta\tilde{Q}^{(2)}_{j,k}}{\Delta\tau^{(2)}} + \frac{\hat{E}^{(2)}_{j+1/2,k} - \hat{E}^{(2)}_{j-1/2,k}}{\Delta\xi^{(2)}} + \frac{\hat{F}^{(2)}_{j,k+1/2} - \hat{F}^{(2)}_{j,k-1/2}}{\Delta\eta^{(2)}} \tag{8}$$

where $\hat{E}$ and $\hat{F}$ are numerical fluxes consistent with the transformed fluxes $\tilde{E}$ and $\tilde{F}$. For an explicit integration scheme, these numerical fluxes are evaluated at the nth time-level, and for a fully implicit scheme they are evaluated at the (n + 1)th time-level.

The explicit zonal scheme consists of the following three steps:

1. Integrate the dependent variables at grid points (of both the grids) that do not belong to the zonal boundary, using equations (7) and (8).

2. Integrate the dependent variables at the zonal-boundary points of one of the zones (say zone 2 of fig. 4), using a scheme that conserves fluxes across the zonal boundary.

3. Obtain the dependent variables at the zonal-boundary points of the other zone (say zone 1 of fig. 4) such that the dependent variables are continuous across the zonal boundary.

The implementation of the first step of the zonal scheme is straightforward. The implementation of the second step is described below. Assume that the zonal-boundary points of zone 2 are to be updated using the finite-difference scheme of equation (8). This calculation requires the fluxes $\hat{F}^{(2)}_{j,1/2}$. These fluxes have to be

calculated such that global conservation is maintained. A typical cell of a zonal-boundary point (j,1) is shown in figure 4, points RSTU. The points R and S are midpoints of the cells they lie in, and the points T and U are obtained as follows. The constant j lines of zone 2 are extrapolated into zone 1 to intersect the line CD (CD corresponds to m = mmax - 1/2 in zone 1 and to k = 1/2 in zone 2). The intersection points have the indices (j,1/2). Point T is midway between the points (j+1,1/2) and (j,1/2), and point U is midway between points (j,1/2) and (j-1,1/2). The global conservation property can be shown to be satisfied if the following relationship is satisfied:

$$\frac{1}{2}\left(\hat{F}^{(2)}_{1,1/2} + \hat{F}^{(2)}_{jmax,1/2}\right) + \sum_{j=2}^{jmax-1} \hat{F}^{(2)}_{j,1/2} = \frac{1}{2}\left(\hat{F}^{(1)}_{1,mmax-1/2} + \hat{F}^{(1)}_{\ell max,mmax-1/2}\right) + \sum_{\ell=2}^{\ell max-1} \hat{F}^{(1)}_{\ell,mmax-1/2} \tag{9}$$

A close examination of equation (9) shows that each side of this equation is nothing but a discrete form of the line integral of the numerical flux F along the line CD in figure 4; the equation itself represents flux conservation across the zonal boundary. Equation (9) is only a necessary condition and is not sufficient to define the fluxes $\hat{F}^{(2)}_{j,1/2}$ in a physically meaningful way.

Assume that the $\hat{F}^{(2)}_{j,1/2}$ are obtained by interpolating the $\hat{F}^{(1)}_{\ell,mmax-1/2}$, that is,

$$\hat{F}^{(2)}_{j,1/2} = \sum_{\ell=p}^{q} N_{j,\ell}\hat{F}^{(1)}_{\ell,mmax-1/2} \tag{10}$$

where the $N_{j,\ell}$ are interpolation coefficients and p and q define the set of points of zone 1 that will be used in the interpolation. We now describe a very simple way of obtaining the interpolation coefficients $N_{j,\ell}$ such that equation (9) is automatically satisfied. Let the line CD in figure 5 correspond to the line CD in figure 4. The dots represent the grid points

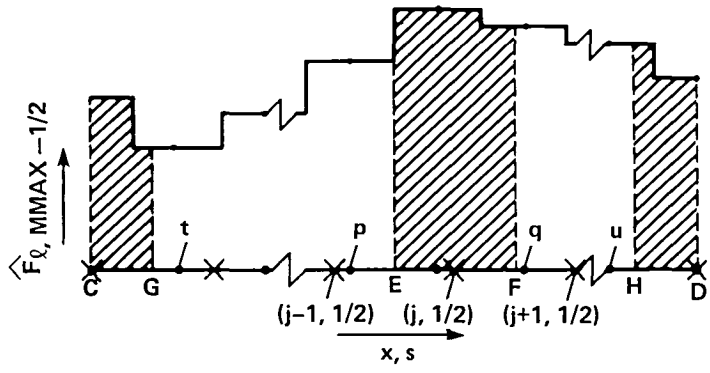

Figure 5.- Piecewise constant variation of the numerical flux $\hat{F}$ as a function of s.

of zone 1 and the crosses represent those of zone 2. A running parameter s is established along the line CD. The quantity s represents the distance of a point from the point C along the curve CD. Representative numerical values of $\hat{F}^{(1)}_{\ell,mmax-1/2}$ are plotted on the positive y-axis. Assume a piecewise constant variation of the numerical fluxes $\hat{F}^{(1)}_{\ell,mmax-1/2}$ along CD, that is $\hat{F}^{(1)}_{\ell,mmax-1/2}$ is constant between $s^{(1)}_{\ell-1/2}$ and $s^{(1)}_{\ell+1/2}$. Consider a point of zone 2, (j,1/2). Let U be midway between (j-1,1/2) and (j,1/2) and T be midway between (j,1/2) and (j+1,1/2). The $\hat{F}^{(2)}_{j,1/2}$ are now calculated from

$$\hat{F}^{(2)}_{j,1/2}(Q,\eta^{(2)}_{j,1/2}) = \int_U^T \frac{\hat{F}^{(1)}_{\ell,mmax-1/2}(Q,\eta^{(1)}_{\ell,mmax-1/2})ds}{(s^{(1)}_{\ell+1/2} - s^{(1)}_{\ell-1/2})}$$

$$= \sum_{\ell=p}^{q} N_{j,\ell}\hat{F}^{(1)}_{\ell,mmax-1/2}(Q,\eta^{(1)}_{\ell,mmax-1/2}) \qquad (11)$$

The end points in the interpolation p and q are shown in figure 5. The treatment of the points (1,1) and (jmax,1) and the calculation of the metrics used in the integration of the zonal points can be found in reference 3.

The final step of the zonal scheme consists of updating the zonal-boundary points of zone 1 such that the dependent variables are continuous across the zonal boundary. This can be done very simply by an interpolation process. The dependent variables at the zonal-boundary points of zone 1 are obtained by interpolating the updated dependent variables at the zonal-boundary points of zone 2. The results in this study were obtained using a linear interpolation scheme.

The Implicit Zonal Scheme

The finite-difference equations (eqs. (7) and (8)) can be made fully implicit by evaluating the numerical fluxes $\hat{E}$ and $\hat{F}$ at the (n + 1)th time-level. However, this results in a system of nonlinear equations that in general need to be solved in an iterative manner. This problem of iteration (and the consequent increase in computing time) is usually circumvented by linearizing the numerical fluxes. The linearization process yields a system of linear equations that can be solved easily using a "block" matrix solver.

In one-dimensional problems, the block matrix resulting from the linearization is tridiagonal, and its inversion is computationally inexpensive. However, in two and three dimensions the matrix is still sparse, but it may have a large bandwidth (depending on the grid-point numbering system). The inversion of the matrix in this case is computationally expensive. To overcome this problem, the left-hand side of the linearized equation is factored (ref. 4). Factorization results in multiple block-tridiagonal matrices on the left-hand side of the equation that need to be inverted sequentially. This approach has a disadvantage in that it introduces a factorization error that increases with increasing step size. In practice, the factorization error makes the scheme conditionally stable (in problems involving strong shocks that move rapidly through the grid, linearization errors could also lead to instabilities at large CFL numbers). Factorization error also reduces the magnitude of the step size at which the fastest convergence is obtained.

Reference 5 presents a Newton-iterative scheme that retains the advantages of the linearization and factorization techniques. The iterative scheme for equation (8) can be written as

$$\left\{I + \frac{\Delta\tau}{\Delta\xi}\left[\nabla_\xi(\tilde{A}^+)^p + \Delta_\xi(\tilde{A}^-)^p\right]\right\}\left\{I + \frac{\Delta\tau}{\Delta\eta}\left[\nabla_\eta(\tilde{B}^+)^p + \Delta_\eta(\tilde{B}^-)^p\right]\right\}\left[(\tilde{Q}^{(2)})^{p+1} - (\tilde{Q}^{(2)})^p\right]$$

$$= -\left[(\tilde{Q}^{(2)})^p - (\tilde{Q}^{(2)})^n\right] - \Delta\tau\left[\frac{\hat{E}^{(2)}_{j+1/2,k} - \hat{E}^{(2)}_{j-1/2,k}}{\Delta\xi} + \frac{\hat{F}^{(2)}_{j,k+1/2} - \hat{F}^{(2)}_{j,k-1/2}}{\Delta\eta}\right]^p \tag{12}$$

where $\tilde{A}^+$, $\tilde{A}^-$, $\tilde{B}^+$, and $\tilde{B}^-$ are Jacobian matrices given by

$$\left.\begin{aligned}\tilde{A}^\pm &= (\tilde{A} \pm |\tilde{A}|)/2\\ \tilde{B}^\pm &= (\tilde{B} \pm |\tilde{B}|)/2\\ \tilde{A} &= \partial\tilde{E}/\partial\tilde{Q}\\ \tilde{B} &= \partial\tilde{F}/\partial\tilde{Q}\end{aligned}\right\} \tag{13}$$

and Δ and ∇ are first-order-accurate forward and backward difference operators. The variable p in equation (12) denotes the iteration number ($\tilde{Q}^p$ is an iterative update of $\tilde{Q}^n$). When $p = 0$, $\tilde{Q}^p = \tilde{Q}^n$, and when equation (12) converges, $\tilde{Q}^p = \tilde{Q}^{n+1}$. Note that the left-hand side of equation (12) becomes zero at convergence for every integration step. This implies that equation (8), with the fluxes evaluated at the $(n + 1)$th level, is satisfied at each integration step. A second point of interest is that the iterative scheme reverts to the noniterative scheme (of the type developed in ref. 4) when only one iteration is performed.

In two dimensions, the iterative approach has the added advantage that the factorization error is driven to zero at each step if the iteration converges. It has also been found that the iterative approach enhances stability (ref. 5); that is, it is possible to use larger CFL numbers than with noniterative schemes. It should be noted that although the iterative approach permits the use of larger CFL numbers, there still exists a CFL limitation because at very large CFL numbers the iteration cycle may not converge owing to factorization error. This problem can be overcome by resorting to relaxation methods that do not require factorization (ref. 6). The primary disadvantage of the iterative approach is the added computation that the iterations require. This is offset to some extent by the larger step sizes that are possible with the iterative scheme.

Noniterative factored schemes require grid lines to be continuous in order to maintain the block-tridiagonal structure of the implicit equations. Since grid lines are not continuous in zonal calculations, noniterative factored schemes are not the most efficient methods for solving the zonal, implicit equations. Iterative schemes are more adaptable to zonal calculations because approximations that restore the block-tridiagonal nature of the matrices can be made. Additionally, these approximations can be corrected for during the iterative process. The details of such an approach are given below.

In implicit zonal calculations it is required to linearize the numerical flux $(\hat{F}^{(2)}_{j,1/2})^{n+1}$ (in addition to the interior fluxes). From equation (11) it is clear that this linearization will take the form

$$(\hat{F}^{(2)}_{j,1/2})^{n+1} = (\hat{F}^{(2)}_{j,1/2})^{n} + \sum_{\ell=p}^{q} N^{n+1}_{j,\ell}(\alpha^{n}_{\ell,mmax-1/2}\ \Delta\tilde{Q}^{(1)}_{\ell,mmax} + \beta^{n}_{\ell,mmax-1/2}\ \Delta\tilde{Q}^{(1)}_{\ell,mmax-1}) \tag{14}$$

where $\alpha^{n}_{\ell,mmax-1/2}$ and $\beta^{n}_{\ell,mmax-1/2}$ are Jacobian matrices given by

$$\left.\begin{aligned} \alpha^{n}_{\ell,mmax-1/2} &= [\partial(\hat{F}^{(1)}_{\ell,mmax-1/2})/\partial\tilde{Q}^{(1)}_{\ell,mmax}] \\ \beta^{n}_{\ell,mmax-1/2} &= [\partial(\hat{F}^{(1)}_{\ell,mmax-1/2})/\partial\tilde{Q}^{(1)}_{\ell,mmax-1}] \end{aligned}\right\} \tag{15}$$

The introduction of the $\Delta\tilde{Q}^{(1)}_{\ell,mmax}$ and $\Delta\tilde{Q}^{(1)}_{\ell,mmax-1}$ into the system of linear equations of zone 2 destroys the block-tridiagonal nature of the system. In order to retain the block-tridiagonal nature of the system the following approximation is made:

$$\Delta Q^{(1)}_{\ell,mmax} \cong \Delta Q^{(2)}_{j,1} \qquad \ell = p \ldots q \tag{16}$$

Equation (16) is a zeroth-order approximation which yields

$$\Delta\tilde{Q}^{(1)}_{\ell,mmax} = \frac{(J^{(2)}_{j,1})^{n+1}}{(J^{(1)}_{\ell,mmax})^{n+1}}\ \Delta\tilde{Q}^{(2)}_{j,1} - \left[1 - \frac{(J^{(1)}_{\ell,mmax})^{n}}{(J^{(1)}_{\ell,mmax})^{n+1}}\right](\tilde{Q}^{(1)}_{\ell,mmax})^{n}$$
$$+ \frac{(J^{(2)}_{j,1})^{n+1}}{(J^{(1)}_{\ell,mmax})^{n+1}}\left[1 - \frac{(J^{(2)}_{j,1})^{n}}{(J^{(2)}_{j,1})^{n+1}}\right](\tilde{Q}^{(2)}_{j,1})^{n} \tag{17}$$

For a stationary grid, equation (17) reduces to

$$\Delta\tilde{Q}^{(1)}_{\ell,mmax} = \frac{(J^{(2)}_{j,1})^{n}}{(J^{(1)}_{\ell,mmax})^{n}}\ \Delta\tilde{Q}^{(2)}_{j,1} \tag{18}$$

Additionally, we make the approximation

$$\Delta\tilde{Q}^{(1)}_{\ell,mmax-1} = 0 \tag{19}$$

Equation (19) is an approximate Dirichlet-type of boundary condition. Equations (18) and (19) together decouple the calculations in the two zones (these approximations are corrected for in the iterative process). Substituting equations (18) and (19) into equation (14) yields

$$(\hat{F}^{(2)}_{j,1/2})^{n+1} = (\hat{F}^{(2)}_{j,1/2})^{n} + \Delta\tilde{Q}^{(2)}_{j,1} \sum_{\ell=p}^{q} N^{n+1}_{j,\ell}\ \alpha^{n}_{\ell,mmax-1/2}\ \frac{(J^{(2)}_{j,1})^{n}}{(J^{(1)}_{\ell,mmax})^{n}} \tag{20}$$

For nonstationary grids, it is necessary to substitute equation (17) instead of equation (18) into equation (14). The use of equation (20) instead of equation (14) to linearize the numerical fluxes at the zonal boundary restores the block-tridiagonal nature of the system.

Equation (13) for the zonal-boundary point (j,1) of zone 2 now takes the form

$$\left\{I + \frac{\Delta\tau}{\Delta\xi}\left[\nabla_\xi(\tilde{A}^+)^p + \Delta_\xi(\tilde{A}^-)^p\right]\right\}$$

$$\times \left\{I + \frac{\Delta\tau}{\Delta\eta}\ \Delta_\eta(\tilde{B}^-)^p + \sum_{\ell=p}^{q} N_{j,\ell}^{n+1}\ \alpha_{\ell,mmax-1/2}^p\ \frac{(J_{j,1}^{(2)})^n}{(J_{\ell,mmax}^{(1)})^n}\right\}\ [(\tilde{Q}^{(2)})^{p+1} - (\tilde{Q}^{(2)})^p]$$

$$= \text{RHS of equation (13)} \qquad (21)$$

Using the approximate linearization of reference 5, $\alpha_{\ell,mmax-1/2}^p$ can now be written as

$$\alpha_{\ell,mmax-1/2}^p = (\tilde{B}_{\ell,mmax}^+)^p \qquad (22)$$

Note that if the zone 1 boundary points were being integrated (instead of interpolated) the $\tilde{B}^-$ terms would come into effect. The interpolation coefficients $N_{j,\ell}^{n+1}$ can be replaced by $N_{j,\ell}^p$ for moving grids. This approximation is not required for stationary grids or for moving grids in which the movement is specified. The approximation vanishes when the solution converges (or, if necessary, at each step, if the iterative process is permitted to converge at each step).

Clearly, equation (20) is only an approximation to equation (14). The inaccuracy in the linearization may lead to inaccuracies in the transient solution (the final converged solution, if one exists, will be the same). However, if the linearization given by equation (20) is used in conjunction with the iterative scheme described earlier (as in eq. (21)), time-accurate results can once again be obtained by iterating equation (12) to convergence at each time-step. This is because the left-hand side is driven to zero at each time-step. The role of the approximate linearization given in equation (20), in the iterative approach, is to merely stabilize the calculation during the iteration process (at CFL numbers greater than that allowed by an explicit scheme). It should also be noted that equation (20) decouples the zone 1 grid points from the zone 2 grid points (at the expense of multiple iterations). This decoupling permits a block-processing approach wherein only the data corresponding to a single zone, or even less, need to reside in the main memory of the computer. The information pertaining to the rest of the zones (except that used for the zonal-boundary condition) may reside on disk or tape memory.

The procedure adopted in this study uses equation (20) in conjunction with the iterative scheme. In practice, only two iterations per time-step were required to perform stable zonal calculations up to CFL numbers of 50.0. At CFL numbers higher than 50.0, instabilities occurred at the surface boundary, and, hence, the zonal boundary condition could not be tested under such conditions.

The implicit zonal scheme can be summarized in the following five steps:

1. Integrate the dependent variables at all the grid points of zone 2, using equation (12) in conjunction with the implicit zonal-boundary condition (eq. (21)) developed earlier (only one iteration).

2. Interpolate the newly obtained values of $[(Q^{(2)}_{j,1})^{p+1} - (Q^{(2)}_{j,1})^{p}]$ along the zonal boundary to yield a new set of values of $[(Q^{(1)}_{\ell,mmax})^{p+1} - (Q^{(1)}_{\ell,mmax})^{p}]$.

3. Integrate the dependent variables at the grid points of zone 1, using equation (12) (only one iteration) and the most recent values of $[(\tilde{Q}^{(1)}_{\ell,mmax})^{p+1} - (\tilde{Q}^{(1)}_{\ell,mmax})^{p}]$ (a Dirichlet-type of boundary condition).

4. Interpolate the values of $(Q^{(2)}_{j,1})^{p+1}$ to obtain the values of $(Q^{(1)}_{\ell,mmax})^{p+1}$ (discard the ones obtained as a result of the integration).

5. If the maximum value of the magnitudes of all $[(\tilde{Q}^{(i)})^{p+1} - (\tilde{Q}^{(i)})^{p}]$ is less than the prescribed tolerance limit, go the next integration step; if not, go back to step 1 and reiterate.

The scheme can be made time-accurate by choosing a sufficiently tight tolerance limit for the iteration cycle. For problems in which only the time-asymptotic solution is required, step 5 may not be necessary. In the demonstration calculation included in this study (cylinder in a supersonic free stream), step 5 was omitted and two iterations were performed at each time-step.

Although a minimum of two iterations is required to perform stable calculations with the zonal technique described above, the second iteration need not be performed at all grid points. In the examples included in this study, it was sufficient to perform the second iteration only at the zonal-boundary points and at one row of points on each side of the zonal boundary. Thus, the extra expense incurred in using an iterative integration scheme as opposed to a noniterative integration scheme is typically less than 20% and decreases as the ratio of the number of zonal points to interior points decreases. A marginal increase in the number of steps to converge may be observed in some cases when the second iteration is performed only in the neighborhood of the zonal boundary.

A Note on Conservation

The iterative implicit zonal scheme (which uses eq. (20) at the zonal boundary) is conservative at each time-step only if the tolerance limit is sufficiently small; otherwise, the scheme is conservative only at convergence (if the problem has a time-asymptotic solution). However, if the zonal fluxes are correctly linearized, as they are in equation (14), then the scheme does not require iteration and is fully conservative at each time-step. The use of equation (14) would require the inversion of a sparse matrix that is not tridiagonal (it would also couple the dependent variables of the different zones). The matrix could be either directly inverted or a relaxation approach could be employed. If a relaxation scheme is used, then the approximate-factorization approach and its attendant problems can be discarded altogether. The relaxation approach to implicit zonal calculations will be presented in a separate article.

INTEGRATION SCHEMES

The results of this study were obtained with the implicit, first-order-accurate and second-order-accurate Osher schemes and the Beam-Warming scheme. This section deals with the evaluation of the numerical fluxes for each of these schemes and with a slight modification that the zonal procedure requires in order to be applicable to the second-order schemes presented here.

Numerical Fluxes for the Integration Schemes

The numerical flux for the first-order-accurate Osher scheme is given by (ref. 7)

$$\hat{E}_{j+1/2,k} = \frac{1}{2}\left[\tilde{E}(Q_{j,k},\xi_{j+1/2,k}) + \tilde{E}(Q_{j+1,k},\xi_{j+1/2,k}) - \Delta E^{+}(Q_{j,k},Q_{j+1,k},\xi_{j+1/2,k}) + \Delta E^{-}(Q_{j,k},Q_{j+1,k},\xi_{j+1/2,k})\right] \tag{23}$$

where

$$\Delta E^{\pm}(Q_{j,k},Q_{j+1,k},\xi_{j+1/2,k}) = \int_{Q_{j,k}}^{Q_{j+1,k}} \left[\frac{\partial \tilde{E}}{\partial Q}(Q,\xi_{j+1/2,k})\right]^{\pm} dQ \tag{24}$$

The numerical flux $\hat{F}_{j,k+1/2}$ can be obtained in a similar manner.

The numerical flux for the second-order-accurate Osher scheme (ref. 7) can be summarized in the following expression:

$$\hat{E}_{j+1/2,k} = \frac{1}{2}\left[\tilde{E}(Q_{j,k},\xi_{j+1/2,k}) + \tilde{E}(Q_{j+1,k},\xi_{j+1/2,k})\right] - \frac{\varepsilon}{2}\left[\Delta E^{+}(Q_{j,k},Q_{j+1,k},\xi_{j+1/2,k}) - \Delta E^{+}(Q_{j-1,k},Q_{j,k},\xi_{j+1/2,k})\right] - \frac{\varepsilon}{2}\left[\Delta E^{-}(Q_{j+1,k},Q_{j+2,k},\xi_{j+1/2,k}) - \Delta E^{-}(Q_{j,k},Q_{j+1,k},\xi_{j+1/2,k})\right] \tag{25}$$

where $\varepsilon = 1.0$ for the Osher scheme. The Beam-Warming scheme (without smoothing) can be obtained by setting $\varepsilon = 0$. For small values of ε, we obtain the Beam-Warming scheme with smoothing, with the smoothing terms possessing an upwind flavor. Additional smoothing terms are not necessary for this form of the Beam-Warming scheme. The values of ε that are usually used are $0.01 < \varepsilon < 0.2$. The upwind smoothing terms consist of both third- and fourth-order terms instead of the conventional purely fourth-order terms. Although the third-order nature of these terms does not affect the formal accuracy of the scheme, this fact should be kept in mind when viscous calculations are performed using the numerical flux of equation (25), because for large values of ε (say $\varepsilon > 0.1$) the truncation error terms may become comparable to the natural viscous terms, thus reducing the accuracy of the calculation. However, small values of ε ($\varepsilon < 0.05$) are sufficient to stabilize the scheme, larger values being required only to damp out the oscillations near shocks. Since ε can be varied over the region of interest without affecting the conservative property of the integration scheme, it is possible to use small values of ε in viscously dominated regions and larger values of ε in regions where shocks are captured.

The Beam-Warming scheme described above has the following advantages:

1. The smoothing terms can be easily made conservative across the zonal boundary since they are part of the numerical flux.

2. It is possible to transition to upwind schemes in a natural way in regions where upwind schemes are more appropriate than central-difference schemes (regions where viscous effects are negligible).

3. It provides a single framework in which both upwind and central-difference schemes can be represented.

However, the disadvantage of using this form of the scheme is that it is computationally more expensive than the conventional form (ref. 4). It should be noted that this additional expense is incurred only in viscously dominated regions where it is preferable to use the conventional scheme with fourth-order smoothing terms.

Modifications to the Zonal Boundary Condition

The procedure of calculating numerical fluxes to update the zonal boundary points requires a minor modification to be applicable to second-order accurate schemes that require a five-point difference molecule in each spatial direction. A close examination of equation (25) will show that in order to calculate $\hat{F}^{(2)}_{3/2,j}$ we first need to determine the quantity $\Delta F^{+}(Q_{j,0},Q_{j,1},\eta_{j,3/2})$. This is achieved simply by extrapolating the constant j lines of zone 2 (see fig. 4) to intersect the line $m = mmax - 1$ in zone 1 (or $k = 0$ in zone 2) instead of terminating the extrapolation at the line CD, which corresponds to $k = 1/2$ or $m = mmax - 1/2$. The values of $Q^{(2)}_{j,0}$ are interpolated from the values of $Q^{(1)}_{\ell,mmax-1}$. A simple linear interpolation was used to obtain the results presented in this paper. A similar extrapolation (but this time into zone 2) is required to obtain the fluxes $\hat{F}^{(1)}_{\ell,mmax-1/2}$. The procedure outlined above does not in any way affect the conservative property of the zonal-boundary condition. The additional flux terms that are required to make the integration scheme second-order accurate are once again perfectly balanced across the zonal boundary.

RESULTS AND DISCUSSION

Results are presented in this section for inviscid, supersonic flow past an 80° segment of a cylinder; for inviscid, subsonic flow past a full cylinder, and for vortex motion through a zonal boundary. The supersonic case demonstrates the increase in convergence rates that can be achieved with implicit zonal techniques and also the quality of solutions that the present zonal scheme yields. The subsonic case demonstrates the time-accuracy of the zonal scheme and the feasibility of performing calculations on zones that move relative to each other. The vortex calculation once again shows the time-accuracy of the zonal scheme and also the distortion-free motion of vortices through zonal boundaries.

Cylinder in a Supersonic Free Stream

The free-stream Mach number for this case of a cylinder in a supersonic free stream was chosen to be 2.0. The dependent variables at all grid points were

initialized to free-stream values. The finite-difference equations together with the various boundary conditions (including the implicit zonal-boundary condition developed in this study) were integrated to convergence. The boundary condition used at the surface of the cylinder is implicit and characteristic in nature. Details of its implementation are given in reference 8.

Two-zone calculation- The grid used for the two-zone calculation is shown in figure 6. The discontinuity of the constant ξ lines along the zonal boundary AB is clearly seen. The bow shock associated with this flow first appears at the surface of the cylinder and then moves outward through the zonal boundary to its converged position in zone 2.

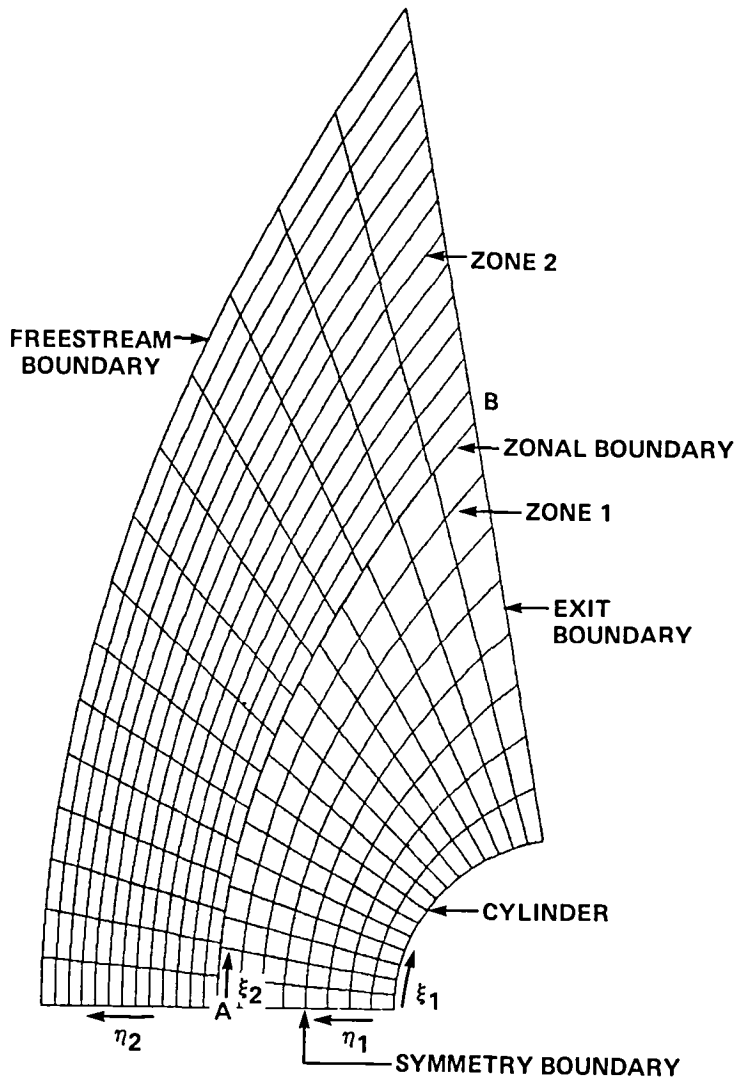

Figure 6.- Grid for two-zone cylinder (supersonic) calculation.

Figure 7 shows the pressure contours obtained after 13 steps with the first-order-accurate, implicit Osher scheme. (The square symbols in figs. 7-10 represent the converged shock position predicted by another numerical approach in ref. 9.) Because of the large transients that occur during the first few steps of the calculation, the CFL number had to be gradually increased from 5.0 to 40.0. Table 1 gives the CFL numbers used at different stages of the calculation. The use of larger CFL numbers during the initial period of large transients resulted in the termination of the calculation, because of nonphysical solutions such as negative density. Figures 8 and 9 show pressure contours obtained after 19 and 24 integration steps, respectively. The shock is seen to be passing through the zonal boundary in figure 8, and, in figure 9 the shock has passed through the zonal boundary. Figure 10 shows the pressure contours obtained at convergence. The contours in figure 10 are slope-continuous across the zonal boundary. This is because of the conservative nature of the zonal boundary condition and also because of the continuity of dependent variables that the zonal scheme enforces.

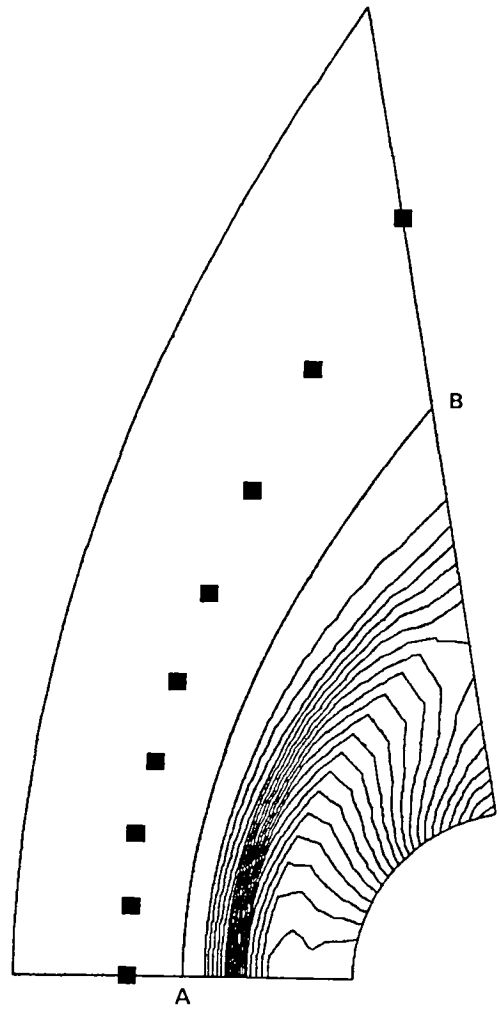

Figure 7.- Isobars after 13 integration steps (first-order Osher scheme).

Figure 11 shows the convergence history for the implicit zonal calculation (with the implicit, first-order-accurate Osher scheme and the implicit zonal-boundary condition) and for an explicit, zonal calculation (with the explicit, first-order-accurate Osher scheme and the explicit zonal-boundary condition). The convergence criterion chosen was

$$|\Delta\rho|_{max} \leq 5\times10^{-4}$$

TABLE 1.- VARIATION OF CFL NUMBER WITH INTEGRATION STEP NUMBER

Integration step (n)	CFL number
$0 < n < 10$	5.00
$10 < n$	40.00

The implicit zonal scheme required 94 steps to converge, whereas the explicit zonal scheme required 2700 steps to converge; that is, the use of the implicit zonal scheme increased the overall convergence rate by a factor of 28.7. However, the implicit scheme with two iterations per time-step (the results shown in figs. 7-11 were obtained with two iterations per time-step) requires 4·8 times as much computing time per time-step as the explicit scheme. Hence, the actual computation cost was reduced by a factor of 6·0 when the implicit zonal scheme was used.

Although two iterations per time-step were used at all the grid points, only the zonal-boundary points and perhaps one or two adjacent rows require multiple iterations (two or more), because of the inaccurate linearization at the zonal boundary. A scheme that takes advantage of this should require less computation time per time-step than a scheme that iterates at all grid points. The two-zone calculation was

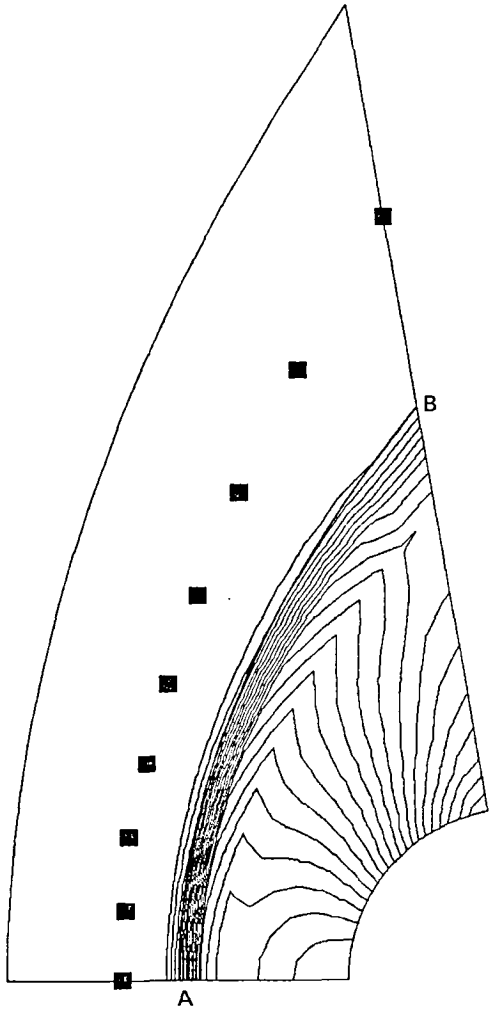

Figure 8.- Isobars after 19 integration steps (first-order Osher scheme).

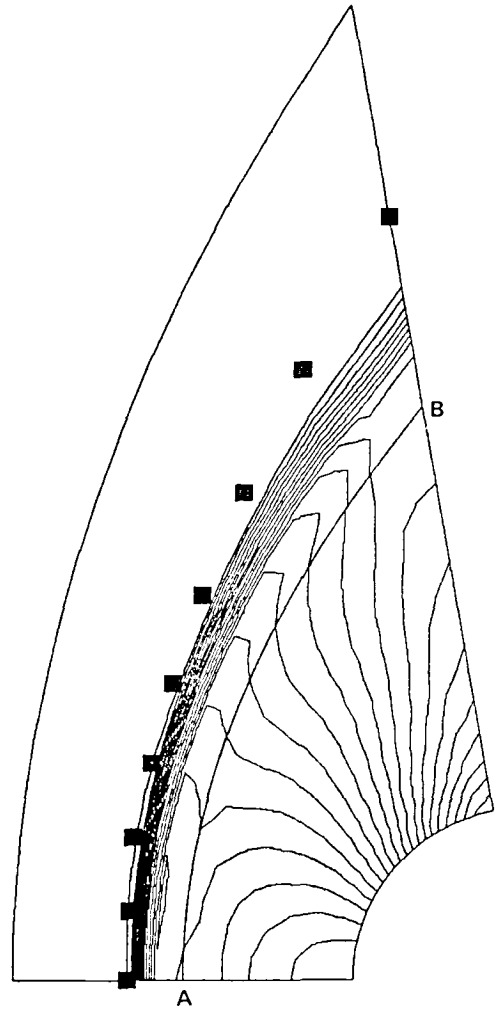

Figure 9.- Isobars after 24 integration steps (first-order Osher scheme).

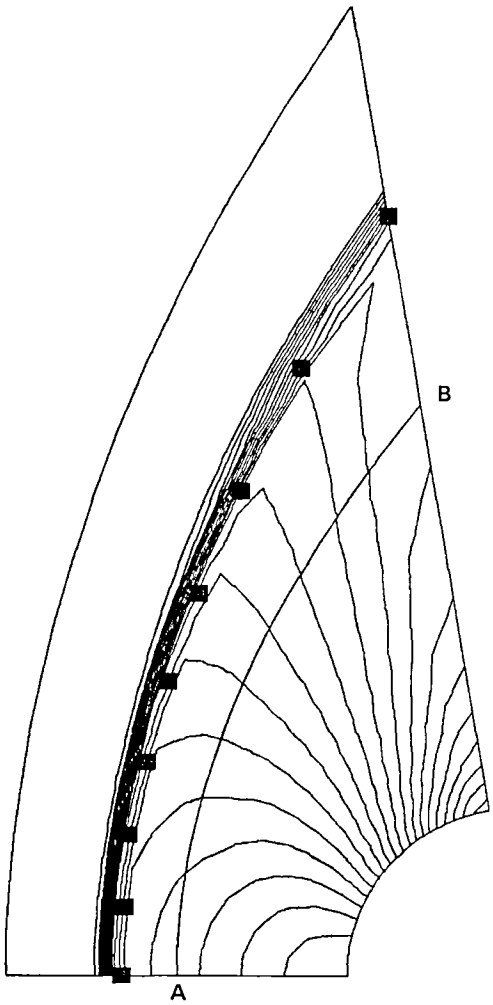

Figure 10.- Isobars at convergence (first-order Osher scheme.

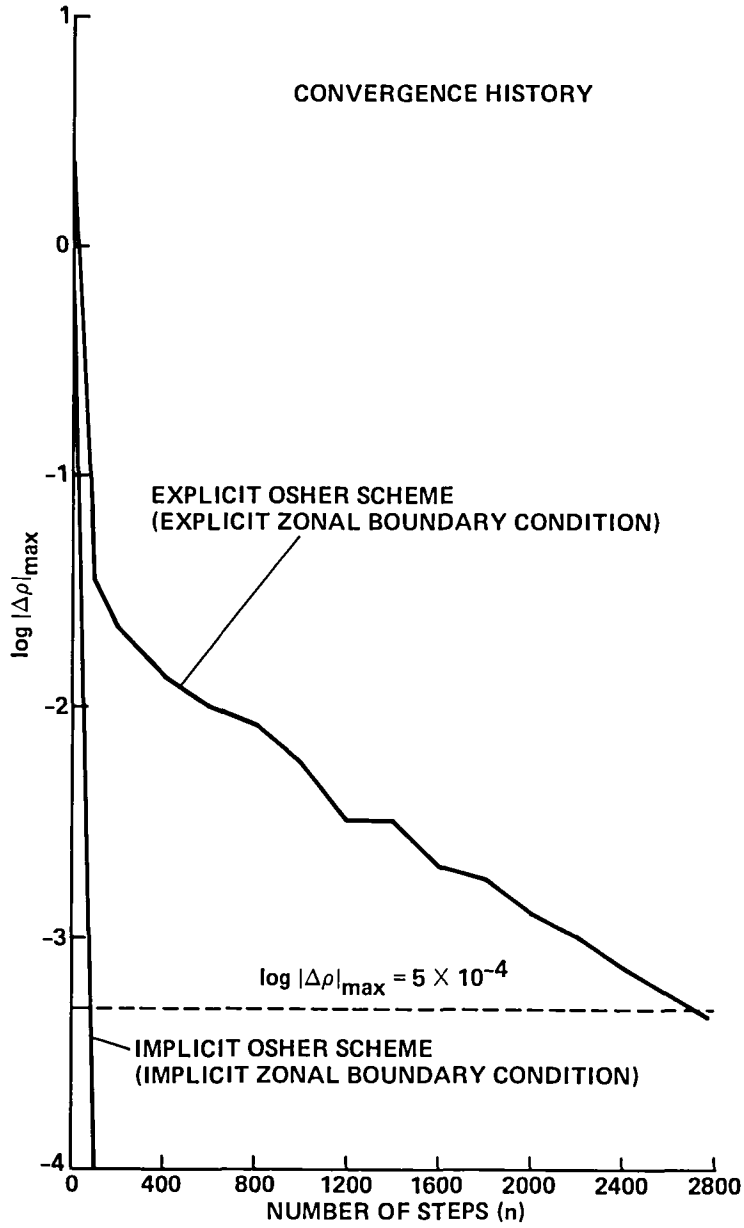

Figure 11.- Convergence history for the cylinder calculation (implicit and explicit first-order Osher scheme calculations).

performed again, with two iterations being used only along the zonal boundary and the row adjacent to it. The CFL number was varied as in the previous case. The calculation was found to be stable but the number of iterations for convergence increased to 122 (a calculation with only one iteration at all grid points was found to be unstable). The computation cost (compared with that for the explicit scheme) was reduced by a factor of 7.3. Table 2 summarizes the computation times and convergence rates for the different approaches mentioned above. All computations were performed on a Cray-XMP.

TABLE 2.- COMPUTATION TIMES FOR FIRST-ORDER-ACCURATE OSHER SCHEME

Computation cost parameters	Number of iterations per step		
	1	2: Second at all points	2: Second on portion of grid
Time per 100 steps, sec	10.55	20.18	12.78
Number of steps to converge	Unstable	94	122
Time to converge, sec	Unstable	18.97	15.59

The linearization of a fully implicit scheme results in the loss of some desirable properties of the scheme (such as monotonicity in the case of the first-order-accurate Osher scheme). This can be seen clearly in figures 8 and 9. The oscillations near the shock are seen even before the shock encounters the zonal boundary. These oscillations grow larger as the shock passes through the boundary and eventually vanish at convergence (fig. 10) as expected (ref. 5). The oscillatory behavior appears because only two iterations per time-step were used instead of the required number of iterations to converge the iteration process at each time-step. To demonstrate the restoration of the properties of the fully implicit scheme (when the iterations converge), the following test was performed. The solution obtained after 22 integration steps (from the previous calculation) was used as the starting solution and integrated through two steps. A CFL number of 40.0 with five iterations per step was used. The residual was reduced by approximately an order of magnitude at the fifth iteration. The pressure contours obtained as a result of this calculation are presented in figure 12. Clearly, the oscillations of figure 9 are absent in figure 12 (figs. 9 and 12 can be directly compared since they show pressure contours at the same time-step). The monotonicity property is restored because at convergence the difference equations corresponding to the fully implicit scheme are satisfied.

Figure 13 displays the pressure contours obtained at convergence with the second-order-accurate Osher scheme. The contours are once again smooth and continuous across the zonal boundary. The second-order accuracy of the method results in oscillatory behavior of the contours near the shock; however, these oscillations are confined to a small region near the shock. The solution required 156 steps to converge when two iterations were performed at all the grid points and 155 steps when two iterations were performed only along the rows adjacent to the zonal boundary. The second-order scheme requires only about 25% more computation time per step than the first-order scheme. The total computation time to obtain the converged second-order solution is

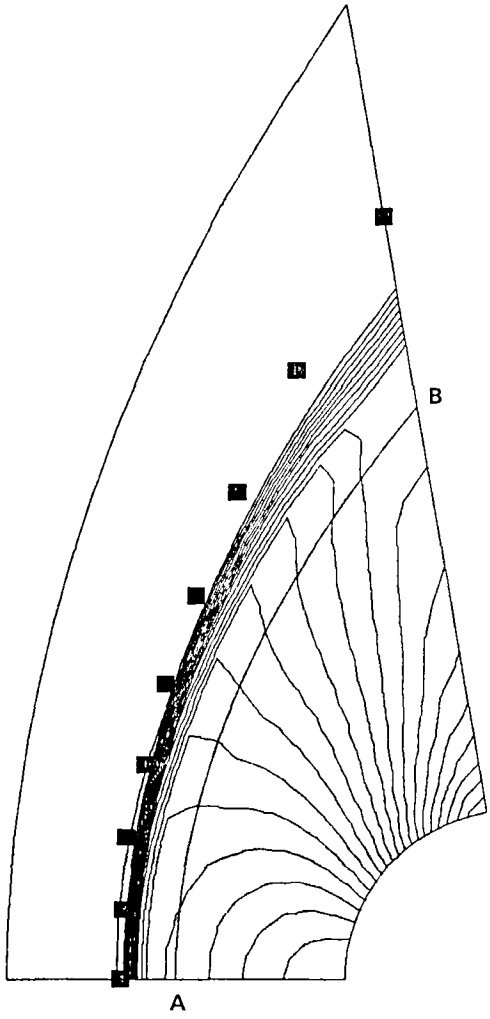

Figure 12.- Isobars after 24 integration steps (the last two steps with 5 iterations per step), using the first-order Osher scheme.

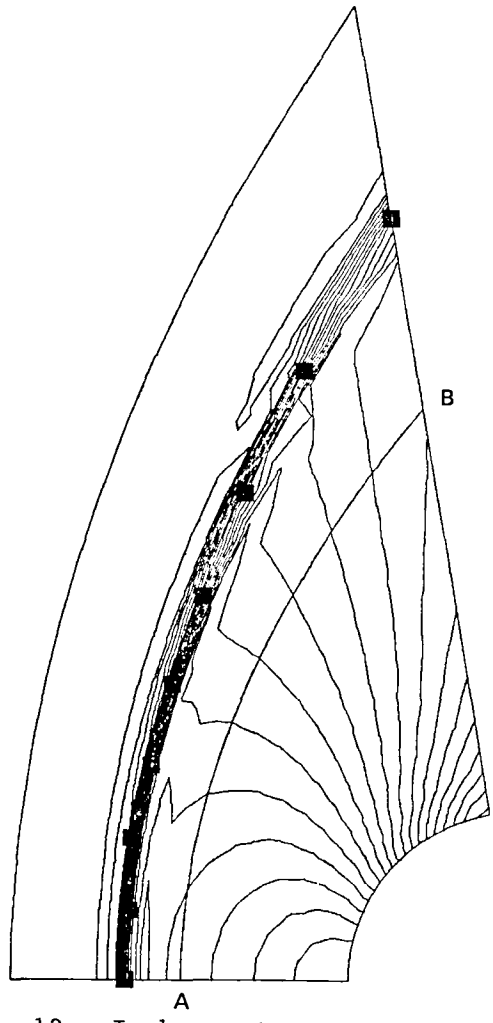

Figure 13.- Isobars at convergence, using the second-order Osher scheme.

about 65% more than that required by the first-order scheme. However, second-order accuracy is essential to building reliable, general-purpose codes. Results obtained with the first-order scheme have been presented merely to demonstrate the increase in convergence speeds and the decrease in computation costs (compared with the results of ref. 3) that are possible with implicit integration and zonal schemes. Table 3 summarizes convergence speeds and computation costs for the second-order-accurate Osher scheme.

Figure 14 shows the pressure contours obtained at convergence with the Beam-Warming scheme ($\varepsilon = 0.2$). The oscillatory behavior of the solution near the shock is evident. Unlike the second-order Osher scheme, the oscillations are not confined to the immediate vicinity of the shock, but extend as far as the zonal boundary. Although the oscillatory behavior seems to be associated with the zonal boundary, in reality it is not a result of the zonal boundary. This assertion is substantiated by the converged pressure contours shown in figure 15 obtained with the Beam-Warming scheme on the single-zone grid shown in figure 16. The oscillations appear once again and are similar to those in figure 14 (in fact the contours of figs. 14 and 15 are superimposable). A summary of convergence speeds and computing times for the Beam-Warming scheme is given in table 4.

TABLE 3.- COMPUTATION TIMES FOR SECOND-ORDER-ACCURATE OSHER SCHEME

Computation cost parameters	Number of iterations per step		
	1	2: Second at all points	2: Second on portion of grid
Time per 100 steps, sec	12.96	24.85	15.86
Number of steps to converge	Unstable	156	155
Time to converge, sec	Unstable	38.76	24.58

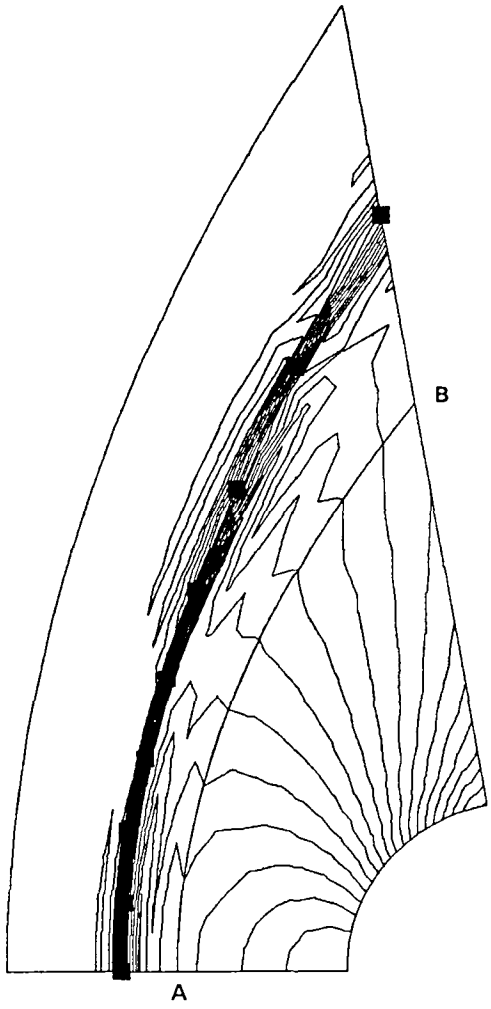

Figure 14.- Isobars at convergence, using the Beam-Warming scheme.

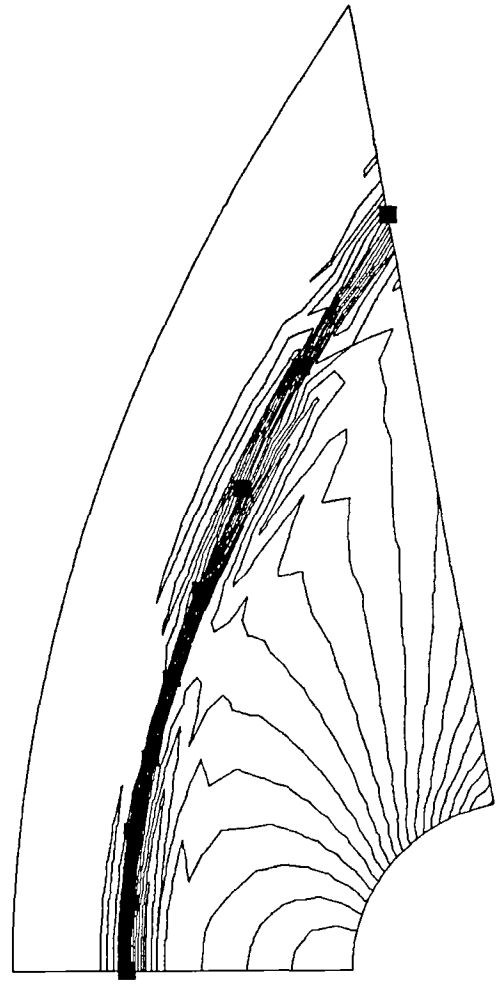

Figure 15.— Isobars at convergence, using the Beam-Warming scheme in conjunction with the grid of figure 16.

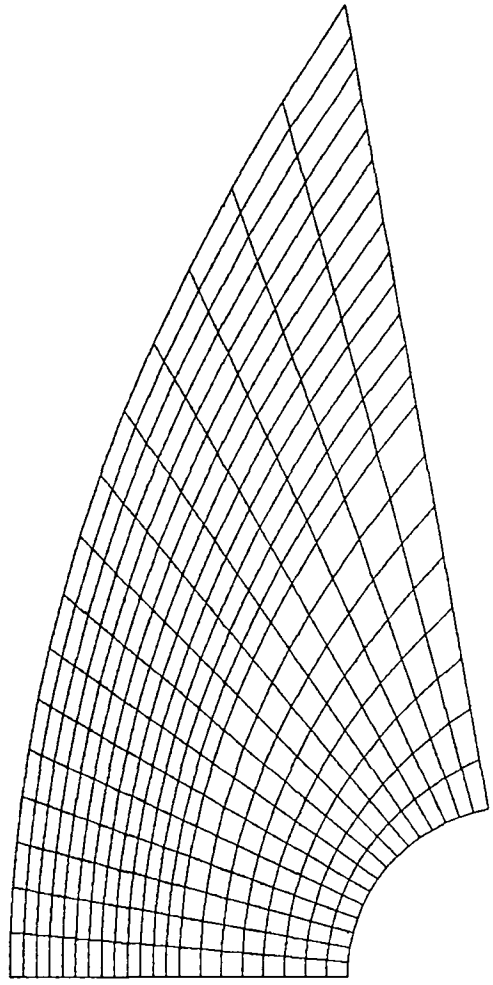

Figure 16.— Grid for one-zone cylinder calculation with the Beam-Warming scheme.

TABLE 4.- COMPUTATION TIMES FOR BEAM-WARMING SCHEME

Computation cost parameters	Number of iterations per step		
	1	2: Second at all points	2: Second on portion of grid
Time per 100 steps, sec	12.96	24.85	15.86
Number of steps to converge	Unstable	104	149
Time to converge, sec	Unstable	25.84	23.63

Some of the oscillations shown in figures 14 and 15 can be removed, without affecting the accuracy of the solution, by adding additional, conventional fourth-order smoothing terms to the grid points in the vicinity of the shock. Such an attempt has not been made in this study. Also, the conventional Beam-Warming scheme requires less computer time per step than that shown in table 4. A conservative zonal scheme that uses the conventional Beam-Warming scheme will be discussed in a separate article.

Four-zone calculation- A general-purpose, zonal Euler code should have the capability of handling as many zones as necessary to cover the region of interest. In order to demonstrate the generality of the present zonal scheme and its applicability in a general-purpose, zonal Euler code, the region of interest for the cylinder was divided into four zones instead of into two zones as was done in the previous case. The zones and the grids for each zone are shown in figure 17. A wide variation in cell shapes and sizes can be seen across each of the three zonal boundaries. Figure 18 shows the pressure contours obtained at convergence with the implicit,

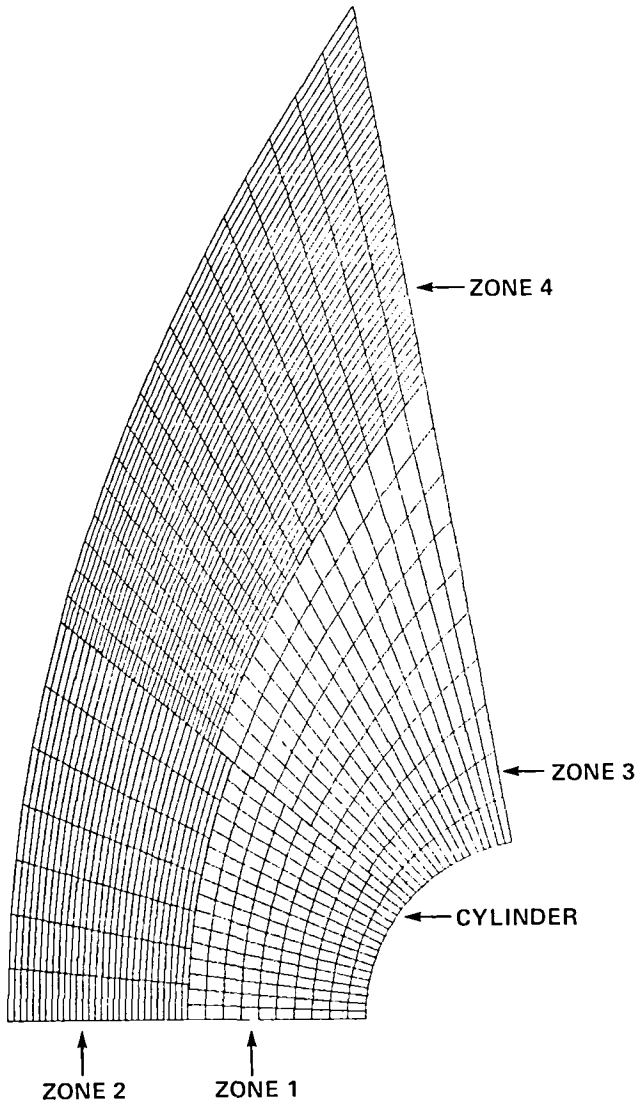

Figure 17.- Grid for four-zone cylinder (supersonic) calculation.

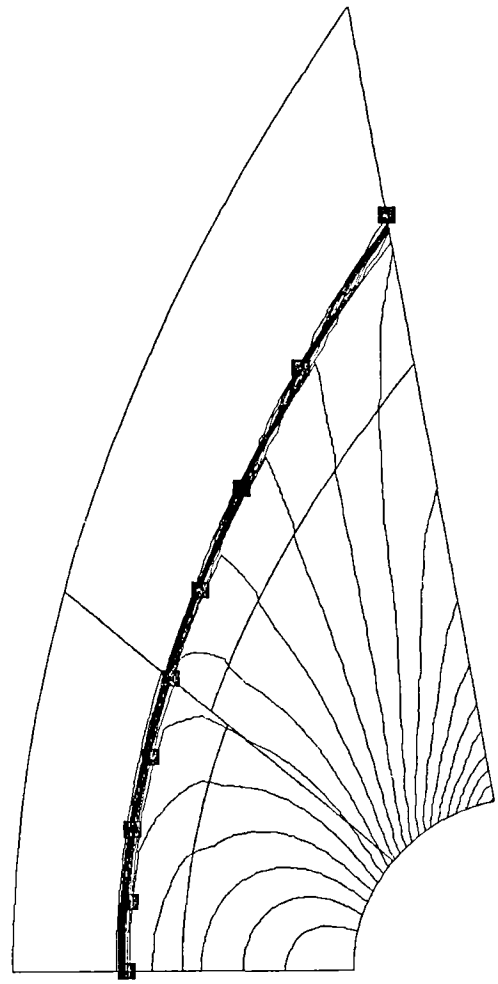

Figure 18.- Isobars at convergence, using the first-order Osher scheme.

first-order-accurate Osher scheme. Small changes in contour line slopes can be seen at the zonal boundaries. This is because of the sudden change in accuracy caused by the abrupt transition in mesh clustering and will be less noticeable for higher-order-accurate schemes. Figures 19 and 20 show the pressure contours obtained with the second-order-accurate Osher and Beam-Warming schemes, respectively. Once again the contours are continuous across the zonal boundaries (and slope continuous unlike the contours in figure 18). The smooth transition of the shock from zone 2 to zone 4 emphasizes the quality of solutions possible with the implicit zonal boundary scheme.

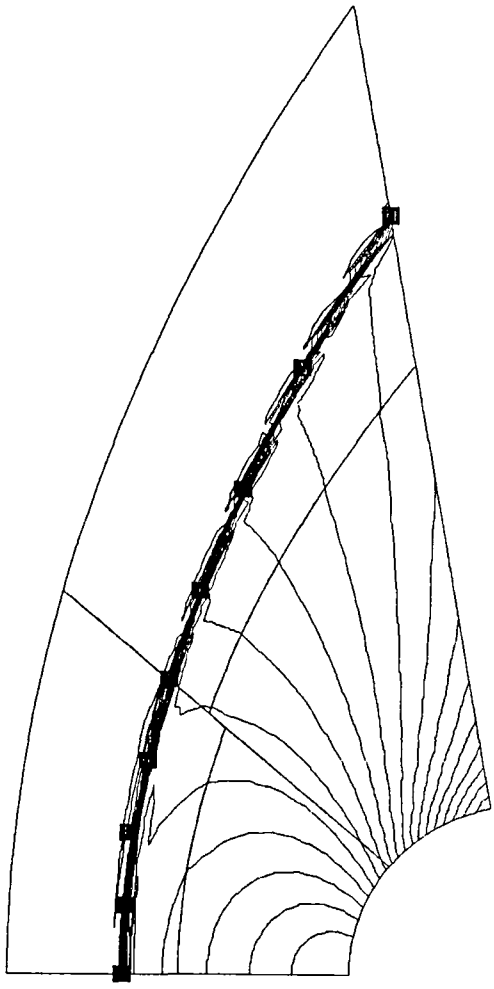

Figure 19.- Isobars at convergence, using the second-order Osher scheme.

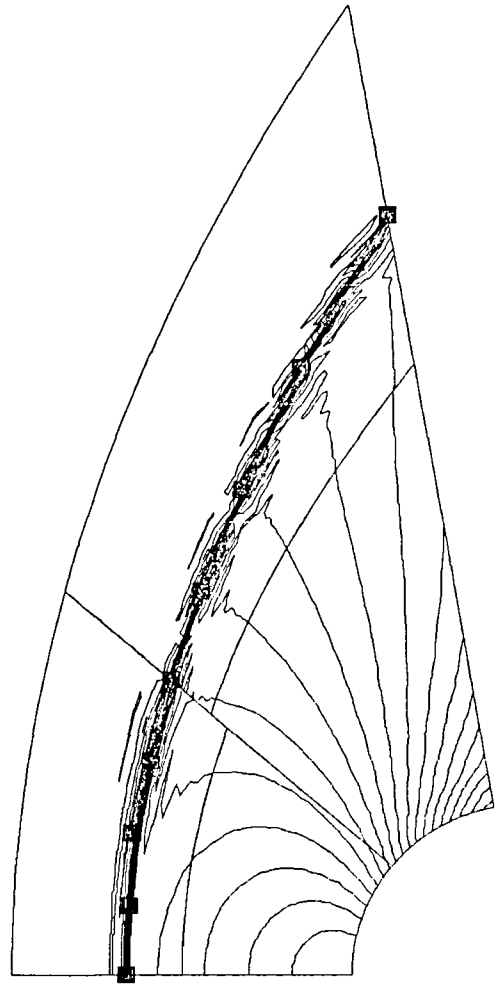

Figure 20.- Isobars at convergence, using the Beam-Warming scheme.

Cylinder in a Subsonic Free Stream (Two-Zone)

The second type of calculation was performed for a complete cylinder in subsonic flow. The free-stream Mach number for this calculation was 0.35; figure 21 shows the two grids used in the calculation. All the grid points were initialized to their free-stream values and the governing equations together with the zonal boundary condition were integrated to convergence (both the grids are stationary for this phase of the calculation). The integration scheme used was the Beam-Warming scheme with $\varepsilon = 0.1$. Second-order accuracy in time was achieved by using a three-point backward difference for the time-derivative on right-hand side of equation (12). The outer

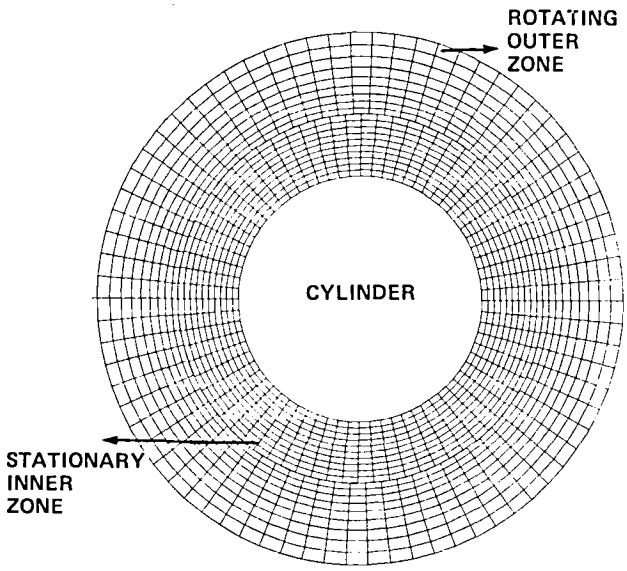

Figure 21.- Grid for two-zone cylinder (subsonic) calculation.

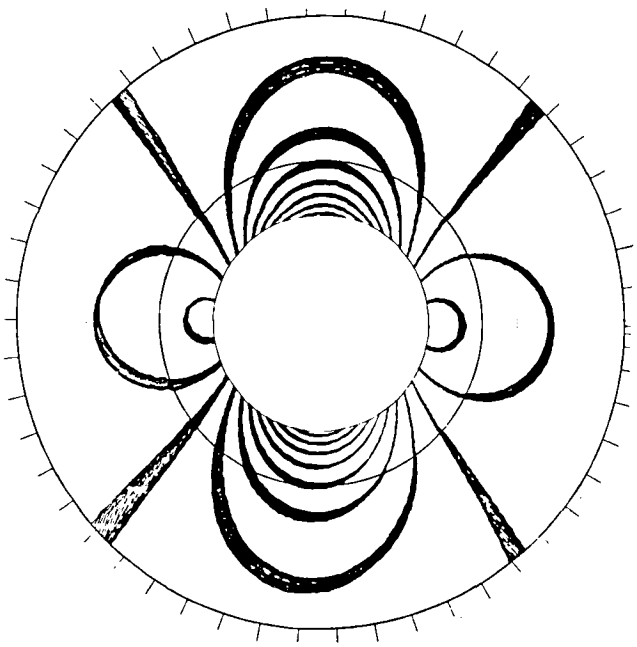

Figure 22.- Isobars at each step as the outer grid performs one rotation.

and then the grid was moved at a constant speed in a direction opposite to the direction in which vortex motion was desired. Figure 23 shows the two-zone grid used for the calculation. Only the central portion of the flow field is presented in figures 23-28, since the essential features of the vortex are contained in this region.

grid was then made to rotate at a constant angular speed. An integration scheme without any truncation error would result in the dependent variables being stationary in physical space and, consequently, contour levels of, for example, pressure and density, would also remain stationary (although in computational space, the dependent variables at a grid point of the outer grid would be constantly changing because of the changing physical location of the grid point).

Figure 22 shows the pressure contours obtained at each time-step, as the outer grid performed one rotation, plotted on the same figure. Two hundred and sixty integration steps were used per rotation. Five iterations were performed at each step in order to reduce the magnitude of the residue by approximately an order of magnitude. For an integration scheme of infinite accuracy, the thickness of the bands would be zero. Since the integration scheme used is only second-order accurate in space and time, the thickness of the contour bands is finite. The thickness of the bands gives a qualitative measure of the time-accuracy of the integration scheme coupled with the zonal scheme. Further details of this calculation are given in reference 10. Reference 10 also includes a demonstration calculation which shows that the finite thickness of the contour bands is a result of the accuracy of the integration scheme and not of any inadequacy in the zonal-boundary scheme.

Vortex Motion through a Zonal Boundary

This calculation consisted of a Lamb-type analytical vortex moving through a zonal boundary. It is possible to effect vortex motion either by superimposing a moving free-stream condition (in which case the vortex is convected along with the fluid at the free-stream velocity) or by keeping the vortex stationary and moving the grid. The two approaches yield identical results. In this study, the vortex was initialized using the procedure given in reference 11,

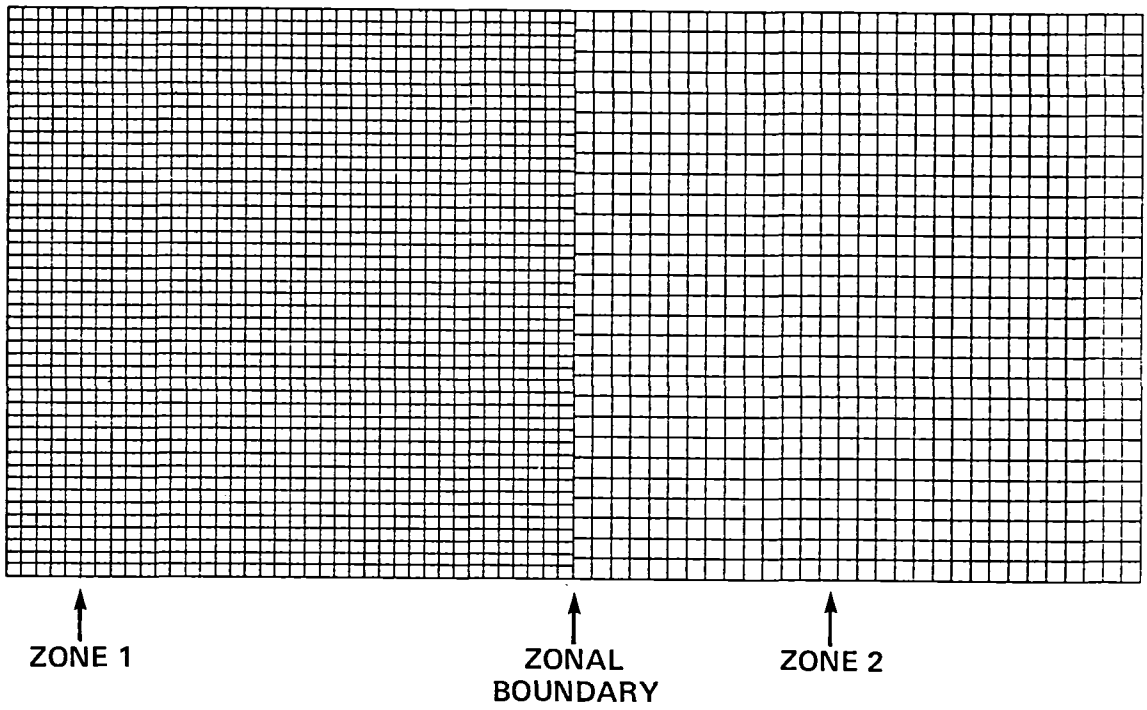

Figure 23.- Grid for two-zone vortex calculation.

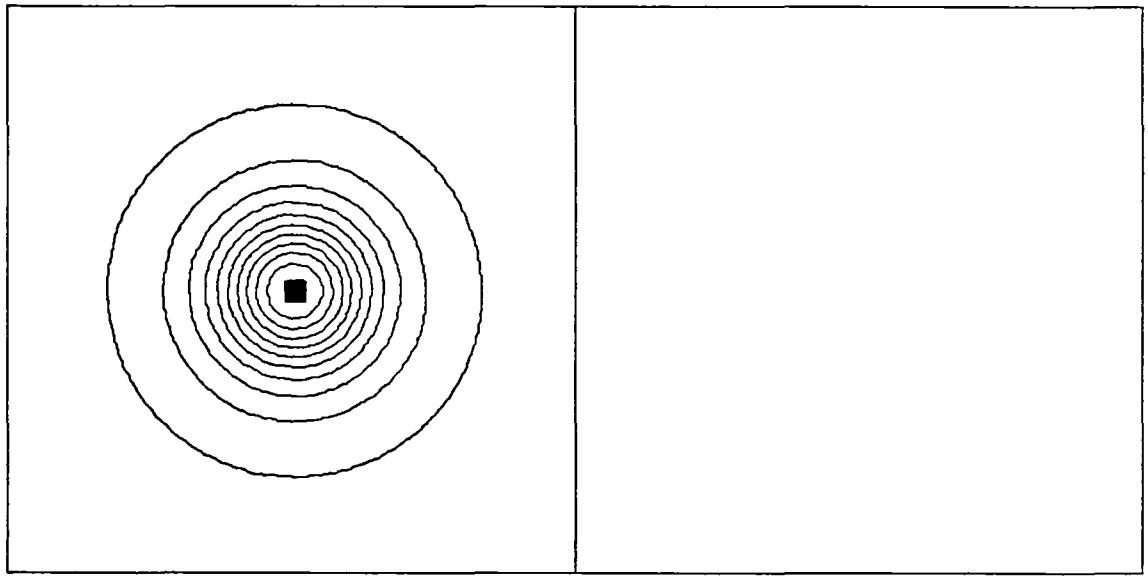

Figure 24.- Isobars for the vortex calculation (at initialization).

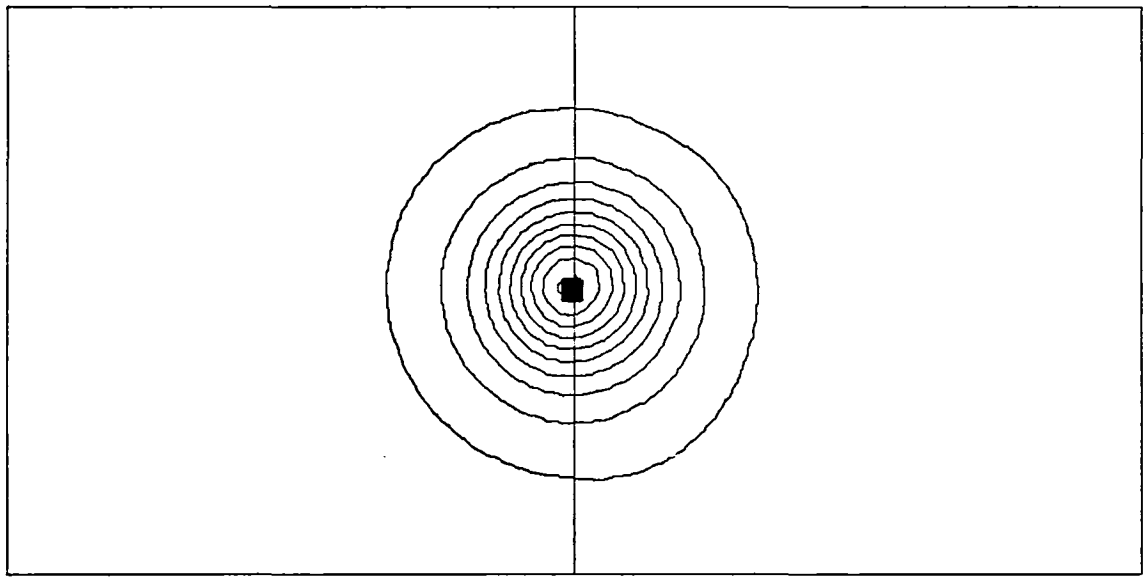

Figure 25.- Isobars for the vortex calculation (after 85 steps).

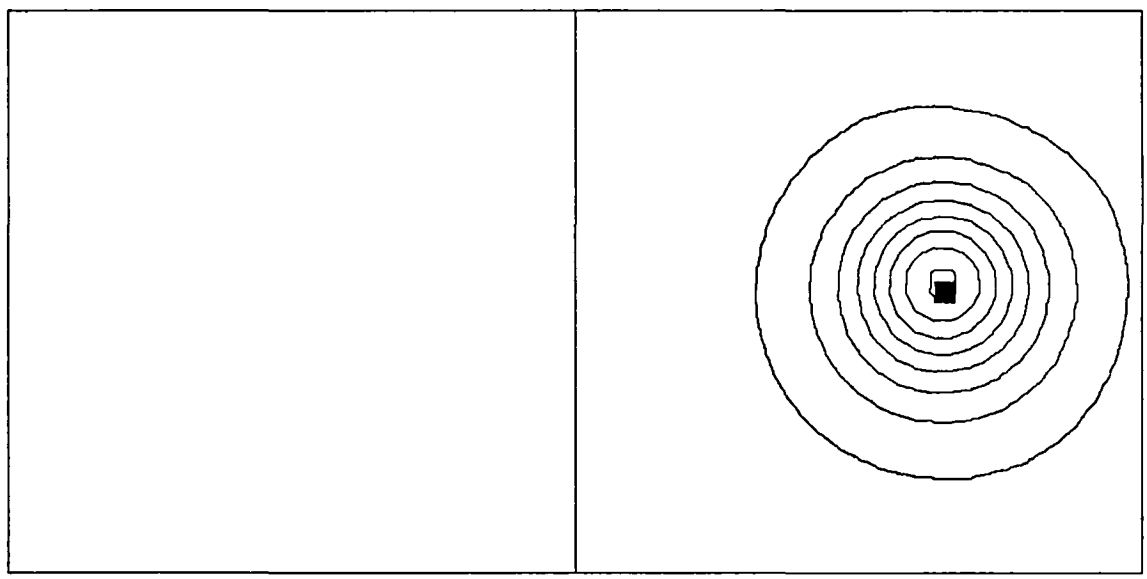

Figure 26.- Isobars for the vortex calculation (after 180 steps).

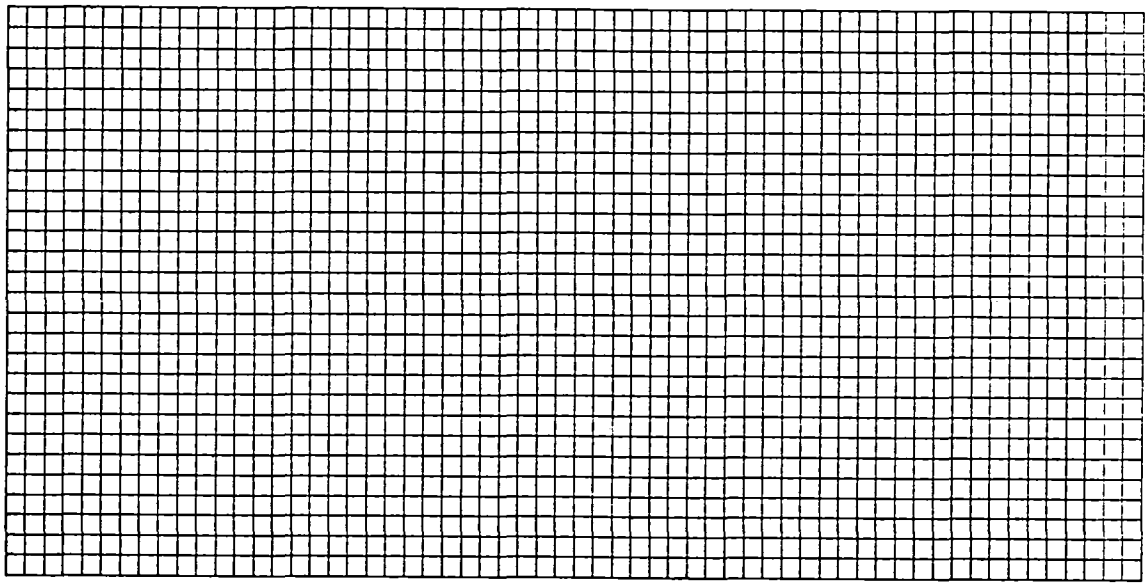

Figure 27.- Grid for single-zone vortex calculation.

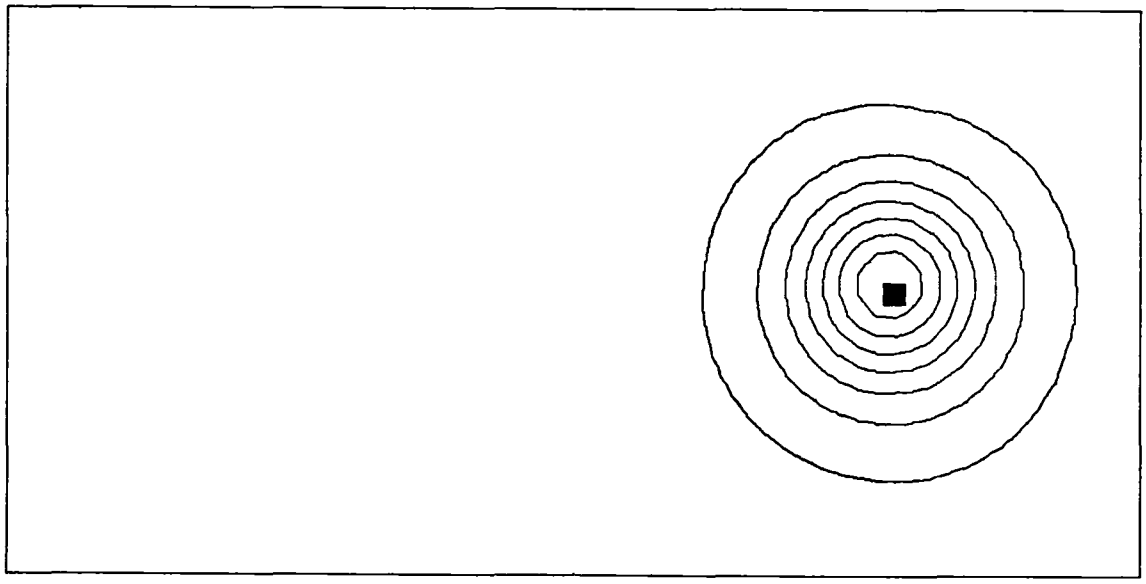

Figure 28.- Isobars for the vortex calculation (after 140 steps).

The discontinuous nature of the grid lines at the zonal boundary is evident. The calculation was performed with the second-order-accurate Osher scheme and three iterations per step. Second-order accuracy in time was achieved as in the previous case.

Figure 24 shows pressure contours at initialization. The solid core at the center of the constant-pressure circles in this figure and the following figures that show pressure contours is the analytical center of the vortex. Figure 25 shows pressure contours after 85 integration steps. The slope continuity of the contour lines across the zonal boundary is clearly seen. The center of the circles coincides with the analytical center of the vortex (this demonstrates the time-accuracy of the zonal scheme). Figure 26 presents pressure contours obtained after 180 integration steps. The vortex has moved entirely into zone 2. The contours are circular and are not distorted. However, because of asymmetric truncation errors, the center of the circles is slightly above the analytical center of the vortex. Figure 27 shows a continuous grid on which the calculation was performed once again. The results of this computation are shown in figure 28 (pressure contours after approximately 140 integration steps). Once again a slight upward movement can be observed, thus demonstrating that this motion is not a result of an inaccurate zonal boundary condition.

CONCLUSIONS

An implicit, conservative zonal-boundary scheme that permits the use of discontinuous zonal grids is developed for the Euler equations. The scheme is an extension of an earlier zonal scheme that was designed for explicit integration schemes. The new implicit scheme can be used with first-order- or second-order-accurate integration schemes. The integration techniques used in this study are the implicit, first-order- and second-order-accurate Osher schemes, and the implicit Beam-Warming scheme. The special logic required to implement the zonal boundary conditions was found to be fairly simple to incorporate in existing codes.

Results in the form of pressure contours are presented for inviscid supersonic flow over a cylinder with the associated bow shock. The calculation was performed on both two-zone and four-zone grid systems. The contours in both cases are observed to be continuous across zonal boundaries, and discontinuities were found to move freely and with minimal distortion through zonal boundaries. The zonal-boundary scheme was found to be stable even under severe test conditions such as strong discontinuities passing through the zonal boundaries at CFL numbers up to 40.0. At this CFL number, the use of the implicit zonal scheme increased the convergence rate by a factor of 28 (over that of the explicit zonal scheme), and the computation cost was reduced by a factor of 7. The results demonstrate the feasibility of efficiently using an implicit zonal approach with discontinuous grids in solving flow problems that involve discontinuous solutions.

Results are also presented for subsonic flow past a cylinder calculated on two grids, one moving and the other stationary. These results demonstrate the time-accuracy of the zonal scheme and the feasibility of calculations on zones that move relative to each other. The ability to perform such calculations should prove useful in solving problems in which some parts of a system are moving relative to each other (e.g., rotor-fuselage combinations). A second problem that demonstrates the time-accuracy of the zonal scheme presented herein consists of a Lamb-type vortex moving through a discontinuous zonal boundary. The movement is distortion-free and time-accurate.

REFERENCES

1. Rai, M. M.; Chaussee, D. S.; and Rizk, Y. M.: Calculation of Viscous Supersonic Flows over Finned Bodies. AIAA Paper 83-1667, Danvers, Mass., 1983.

2. Rai, M. M.; Chakravarthy, S. R.; and Hessenius, K. A.: Metric-Discontinuous Zonal Grid Calculations Using the Osher Scheme. To appear in the International Journal of Computers and Fluids.

3. Rai, M. M.: A Conservative Treatment of Zonal Boundaries for Euler Equation Calculations. AIAA Paper 84-0164, Reno, Nev., 1984.

4. Beam, R. M.; and Warming, R. F.: An Implicit Factored Scheme for the Compressible Navier-Stokes Equations. Proceedings of the AIAA 3rd Computational Fluid Dynamics Conference, Albuquerque, N. Mex., June 27-28, 1977.

5. Rai, M. M.; and Chakravarthy, S. R.: An Implicit Form for the Osher Upwind Scheme. AIAA Paper 84-0088, Reno, Nev., 1984.

6. Chakravarthy, S. R.: Implicit Upwind Schemes without Approximate Factorization. AIAA Paper 84-0165, Reno, Nev., 1984.

7. Chakravarthy, S. R.; and Osher, S.: High Resolution Applications of the Osher Upwind Scheme for the Euler Equations. AIAA Paper 83-1943, Danvers, Mass., 1983.

8. Rai, M. M.; and Chaussee, D. S.: New Implicit Boundary Procedures: Theory and Application. AIAA Paper 83-0123, Reno, Nev., 1983.

9. Lyubimov, A. N.; and Rusanov, V. V.: Gas Flows past Blunt Bodies. NASA TT-F 715, 1973.

10. Hessenius, K. A.; and Rai, M. M.: Applications of a Conservative Zonal Scheme to Transient and Geometrically Complex Problems. AIAA Paper 84-1532, Snowmass, Colo., 1984.

11. Srinivasan, G. R.; McCroskey, W. J.; and Kutler, P.: Numerical Simulation of the Interaction of a Vortex with Stationary Airfoil in Transonic Flow. AIAA Paper 84-0254, Reno, Nev., 1984.

1. Report No.	2. Government Accession No.	3. Recipient's Catalog No.
NASA CR-3865		

4. Title and Subtitle	5. Report Date
AN IMPLICIT, CONSERVATIVE, ZONAL-BOUNDARY SCHEME FOR EULER EQUATION CALCULATIONS	February 1985
	6. Performing Organization Code

7. Author(s)	8. Performing Organization Report No.
Man Mohan Rai	A-9823
	10. Work Unit No.
	T-6458

9. Performing Organization Name and Address	11. Contract or Grant No.
Informatics General Corporation Palo Alto, California 94303	NAS2-11555
	13. Type of Report and Period Covered
	Contractor Report

12. Sponsoring Agency Name and Address	14. Sponsoring Agency Code
National Aeronautics and Space Administration Washington, DC 20546	505-31-01-01-00-21

15. Supplementary Notes

Point of Contact: M. M. Rai, Ames Research Center, MS 202A-14, Moffett Field, CA 94035 (415) 965-6742 or FTS 448-6742

16. Abstract

A "zonal," or "patched," grid approach is one in which the flow region of interest is divided into subregions which are then discretized independently, using existing grid generators. The equations of motion are integrated in each subregion in conjunction with zonal-boundary schemes which allow proper information transfer across interfaces that separate subregions. The zonal approach greatly simplifies the treatment of complex geometries and also the addition of grid points to selected regions of the flow. In this study a conservative, zonal-boundary condition that could be used with explicit schemes has been extended so that it can be used with existing second-order-accurate implicit integration schemes such as the Beam-Warming and Osher schemes. In the test case considered, the implicit schemes increased the rate of convergence considerably (by a factor of about 30 over that of the explicit scheme). Results demonstrating the time-accuracy of the zonal scheme and the feasibility of performing calculations on zones that move relative to each other are also presented.

17. Key Words (Suggested by Author(s))	18. Distribution Statement
Computational fluid mechanics Grid generation Zonal methods	Unclassified - Unlimited Subject Category - 34

19. Security Classif. (of this report)	20. Security Classif. (of this page)	21. No. of Pages	22. Price
Unclassified	Unclassified	34	A03

For sale by the National Technical Information Service, Springfield, Virginia 22161

NASA-Langley, 1985

National Aeronautics and
Space Administration

Washington, D.C.
20546

Official Business
Penalty for Private Use, $300

THIRD-CLASS BULK RATE

Postage and Fees Paid
National Aeronautics and
Space Administration
NASA-451

U.S.MAIL

NASA

POSTMASTER: If Undeliverable (Section 158
Postal Manual) Do Not Return